QUANTITATIVE ASSESSMENT OF THE HUMAN PHARYNX BASED ON CONE BEAM COMPUTED TOMOGRAPHY

A THESIS SUBMITTED TO THE GRADUATE DIVISION OF THE UNIVERSITY OF HAWAI`I AT MĀNOA IN PARTIAL FULFILLMENT OF THE REQUIREMENTS FOR THE DEGREE OF

MASTER OF SCIENCE

IN

DEVELOPMENTAL AND REPRODUCTIVE BIOLOGY

DECEMBER 2011

By

Karra S.H. Imoto

Thesis Committee:

Dr. Scott Lozanoff, Chairperson
Dr. Vernadeth Alarcon
Dr. Cristopher D. Stickley

ACKNOWLEDGEMENTS

Deepest thanks to Dr. Scott Lozanoff, Committee Chairman, for his advice and support from the beginning to completion of this project. I am grateful for his constant encouragement and guidance in my development and understanding of this subject.

Also, thank you to committee members Dr. Vernadeth Alarcon and Dr. Cris Stickley for their insights and guidance.

This thesis would not have been possible without the generous collaboration of Dr. Neil Norton, School of Dentistry Creighton University who provided the cone beam computed tomography images for analysis.

Lastly, I am indebted to the many colleagues and department faculty who supported me throughout this project.

ABSTRACT

Three-dimensional imaging is a rapidly developing area useful for visualizing pharyngeal morphology. The purpose of this study is to implement and validate Airway3D computer software for generating 3D human- airway models from cone-beam computed tomography and to quantify pharyngeal sizes and shapes. This was accomplished by assessing Airway3D's boundary-extraction efficiency, the accuracy of 3D airway models, and the utilization of conventional cephalometric (CCA) and geometric morphometric analyses (GMA). Twenty male and female Digital Imaging in Communications and Medicine (DICOM) formatted volume images were randomly selected from a pre-existing database. Three-dimensional models were automatically generated, digitization was performed, and both processes were assessed for accuracy and reliability. Landmarked 3D models were qualitatively and quantitatively compared between genders, and CCA results were used to validate developing dense-correspondence analysis available. Results showed that Airway3D produced valid 3D models and accurate CCA and GMA. It is concluded that Airway3D can be used to effectively partition pharyngeal morphology into separate and quantifiable measures of size and shape.

TABLE OF CONTENTS

ACKNOWLEDGEMENTS iii

ABSTRACT iv

LIST OF TABLES vii

LIST OF FIGURES viii

LIST OF ABBREVIATIONS x

CHAPTER 1. INTRODUCTION 1

Background 1

The Pharynx 1

The Pharynx in Obstructive Sleep Apnea 2

Diagnosis of OSA 3

Treatment of OSA 4

Dental Treatment and Cephalometric Assessment 4

Cone Beam Computed Tomography and Imaging 6

Airway3D Software 8

Specific Aims 9

CHAPTER 2. MATERIALS AND METHODS 11

Design 11

Subjects 11

Procedure 12

Specific Aim 1. Airway Extraction 12

Specific Aim 2. 3D Model Accuracy and Landmark Reliability 13

Specific Aim 3. Geometric Morphometric Analyses 14

CHAPTER 3. RESULTS 17

Specific Aim 1. Airway Extraction 17

Specific Aim 2. 3D Model Accuracy and Landmark Reliability 18

Specific Aim 3. Geometric Morphometric Analyses 18
CHAPTER 4. DISCUSSION 21
Specific Aim 1. Airway Extraction 21
Specific Aim 2. 3D Model Accuracy and Landmark Reliability 21
Specific Aim 3. Geometric Morphometric Analyses 22
CHAPTER 5. CONCLUSIONS AND FUTURE WORK 26
APPENDIX A. TABLES 28
APPENDIX B. FIGURES 35
REFERENCES 57

LIST OF TABLES

Table 1. Anatomical Landmarks for the Airway Model of Nasopharynx to EB..... 28

Table 2. Definitions for Size- Airway Parameters 29

Table 3. Scaled, shape residual for replicates and groups of females and males..... 30

Table 4. Size- Airway Parameters 31

Table 5. CCA Intra-examiner Variability..... 32

Table 6. Size and shape residual for females and males 33

Table 7. DCA for Size and Shape..... 34

LIST OF FIGURES

Figure 1. Automatic airway boundary- extraction of Airway3D 35

Figure 2. User-defined airway boundaries 36

Figure 3. Automatic airway segmentation of Airway3D 37

Figure 4. Gaussian Filter smoothing 38

Figure 5. Landmarks manually identified on CBCT scans 39

Figure 6. Individual female and male segmented volumes 40

Figure 7. Gaussian Filter smoothing from levels 2 through 10 41

Figure 8. Representative female and male airway models 42

Figure 9. Procrustes Superimposition for user reliability 43

Figure 10. Srfit results of Procrustes Superimposition for user reliability 44

Figure 11. Gsf of shape within a female and male 45

Figure 12. PCA table of Male 9 linear measurements 46

Figure 13. Graphs of PCA Axes 1 to 2 and 3 comparing females to males 47

Figure 14. Average female and male airway segmented volumes 48

Figure 15. Average male and female airway volume at threshold 49

Figure 16. PCA Table of replicate F7 to replicate M1 50

Figure 17. PCA plot of PCA axes 1 and 2 comparing replicate F7 to replicate M1 51

Figure 18. PCA Table of females and males 52

Figure 19. Graphs of PCA Axes 1 to 2 and 3 comparing females to males..... 53

Figure 20. Procrustes Superimposition comparing females to males..... 54

Figure 21. Gsf of size and shape between females and males 55

Figure 22. DCA of a female into a male..... 56

LIST OF ABBREVIATIONS

ANOVA	Analysis of variance
CBCT	Cone Beam Computed Tomography
CCA	Conventional cephalometric analysis
CPAP	Continuous positive airway pressure
CPU	Central processing unit
CUDA	Computing unified device architecture
DCA	Dense Correspondence analysis
DICOM	Digital imaging and communications in medicine
EB	Base of the epiglottis
ET	Tip of the epiglottis
GF	Gaussian Filter
GMA	Geometric morphometric analysis
GPU	Graphics processing unit
HP	Hard palate
INC	Inferior nasal conchae
NP	Nasopharynx
OP	Oropharynx
OSA	Obstructive Sleep Apnea
PAP	Positive airway pressure
PCA	Principle Components analysis
PS	Procrustes Superimposition
PSG	Polysomnography
PRM	Portable respiratory monitoring
SPSS	Statistical Package for the Social Sciences

TPS	Thin Plate Spline analysis

CHAPTER 1. INTRODUCTION

Background

The Pharynx

The human pharynx is a vital anatomical structure in the head and neck that is continuous rostrally with the nasal and oral cavities and caudally with the larynx and esophagus. This structure is divisible into the (1) nasopharynx (NP), the cavity behind the soft palate; (2) oropharynx (OP), along the soft palate to the tip of the epiglottis; and (3) laryngopharynx or hypopharynx, from the tip, or most posterior, of the epiglottis to inferior cricoid cartilage, from the base of the skull, sphenoid and occipital bones to cervical vertebrae six (Isaacs & Sykes, 2002). It contributes equally to the digestive and respiratory systems. With respect to the respiratory system, it constitutes the majority of the upper respiratory tract, also known as the upper airway. This portion of the respiratory system is generally considered to be the region rostral to the glottis or vocal cords. The pharynx consists of a distensible muscular tube lined with a relatively thick mucosa with the muscle comprised of walls that are highly diverse in structure, function and nerve innervation. Three pharyngeal constrictor muscles, superior, middle, and inferior muscles, insert posteriorly into a median raphe and anteriorly to the base of the skull, hyoid bone, and cricoid cartilage (Isaacs & Sykes, 2002). Thus, pharyngeal morphology is well known, but its patency is highly variable and depends on integrative functions. Importantly, the pharynx is a frequent site of infection and disease owing to its dual role in the digestive and respiratory systems (Richardson, 2011). In addition, its size and shape largely depends on the state of contracture, and thus nerve innervation, of the diverse set of muscles comprising its wall. Pharyngeal patency depends, at least in part, on musculature activation. Muscle groups shown to maintain pharyngeal patency include hyoid muscles (mylohyoid and geniohyoid), soft palate muscles (levator veli palatine and tensor veli palatini), pharyngeal constrictor muscles, and intrinsic (verticalis, transversus, superior longitudinalis) and extrinsic (genioglossus, hyoglossus, and styloglossus) tongue muscles (Bailey and Fregosi, 2006; Bailey et al., 2006).

The large variety of muscles complicates our understanding of pharyngeal function. As a result, many studies restrict analysis to individual muscles. For example, the contribution to pharyngeal patency by the genioglossus muscle has been examined extensively since it contributes to the anterior pharyngeal wall and thus is easily accessible for analysis (Bailey, 2011). It has been reported that contraction of the genioglossus muscle during tongue protrusion increases OP size and decreases pharyngeal negative pressure, but does not affect pharyngeal stiffness or severity of sleep apnea (Oliven et al., 2007). Thus, pharyngeal morphology may be altered by a single muscle, but pharyngeal stiffness may be due to activation of single muscle units innervating multiple muscles simultaneously (Bailey, 2011). Compromised compliancy and reduced stiffness of the pharynx result in pharyngeal collapse, which can have profoundly negative effects on airway functions, particularly during sleep (Wellman et al., 2011). Thus, assessment of overall pharyngeal size and shape determined by multiple muscles is critical to assessment and diagnosis of function and disease rather than focusing on individual muscle activity. Methods to examine overall morphology of the pharynx in disease states should provide useful information for prevention and treatment.

The Pharynx in Obstructive Sleep Apnea

The pharynx is susceptible to many diseases with unknown mechanisms that alter pharyngeal size and shape complicating our ability to visualize the pharynx with current technologies. One such disease is Obstructive Sleep Apnea, OSA, which is characterized by "repetitive episodes of upper airway obstruction and cessation of breathing that occurs during sleep that may be accompanied by loud snores and brief gasps" (American Academy, 2001). Patients experience excessive daytime sleepiness resulting from recurrent arousals due to these disordered breathing events and sleep fragmentation (Caples et al., 2005). OSA is a major health problem in the United States similar to diabetes in terms of the number of people affected, their economic burdens, and patient suffering (AlGahanim et al., 2008). Prevalence of OSA in the general population is approximately 24% for men and 9% for women with an estimated 12-18 million people affected nationally, costing 15.9 billion dollars annually (Young et al., 2009; Sjosten

et al., 2009). The prevalence of OSA appears positively correlated with increasing trends of obesity (Young et al., 2004), and increased size of neck circumference (Yucel et al., 2005). OSA appears to correlate with a decrease in airway volume (Ogawa et al., 2007; Shigeta et al., 2008; Shigeta et al., 2008) and cross-sectional area (Walsh et al., 2008). It is also linked to increased blood pressure, depression, and mortality as well as an increased occurrence of stroke (Young et al., 2009; Dyken & Im, 2009; Lopez-Jimenez et al., 2008). The estimated economic burden of OSA exceeds that of asthma and chronic obstructive pulmonary disease combined (AlGhanim, 2008).

Unfortunately, the underlying mechanisms of OSA remain unknown, but it has been shown that hypertrophy of pharyngeal tonsils, also known as adenoids, can cause nasal airway obstruction (Isaacs & Sykes, 2002), and during sleep, the neural activation of dilator pharyngeal muscles is attenuated, pharyngeal intraluminal negative pressure increases, and thus airway collapse occurs (Bailey, 2011; Lopez-Jimenez et al., 2008; Oliven et al., 2007). OSA is also accompanied by narrowing of the upper airway (Togeiro et al., 2010) and lateral pharyngeal walls, and enlargement of palatine tonsils, uvula, and tongue (Maria et al., 2010). Recent evidence suggest that “architecture of the oropharynx may also contribute to the development of OSA” (Tso et al., 2009). Many studies include comparisons of non-diseased patients to OSA patients, without standardized normal values. Further analysis and standardization of the size and shape of the airway are necessary to gain a better understanding of anatomical changes due to this disease.

Diagnosis of OSA

Nocturnal pulse oximetry is used as an initial test for OSA (Caples et al., 2005) while polysomnography (PSG) is the standard OSA diagnostic procedure for assessing patients since it provides physiological measures during sleep including oxygen saturation, blood pressure, electromyography for ventilation, sympathetic neural activity, electroencephalography, and nasal airflow (Caples et al., 2010; Kuna, 2010). The method itself disrupts sleep in some patients, confounding the diagnosis (Oda et al., 2003) with experts disagreeing on the diagnostic threshold

at which OSA is indicated (Ahmadi et al., 2008). Diagnosis of OSA is performed in a sleep laboratory, but it is very expensive and many patients without health insurance have no access to assessment or treatment (Kuna, 2010). Portable respiratory monitoring (PRM) is currently being investigated as a tool for diagnosing OSA at home. Portable tests are more economical for initial tests assessing patients suspected OSA (Ayas et al., 2010). Even if available, diagnostic and assessment protocols for OSA remain expensive, imprecise and insufficient to achieve optimal treatment outcomes for many patients. Thus one diagnostic option is not sufficient to accurately assess the airway, and other methods are thus necessary.

Treatment of OSA

Treatments for OSA patients general health considerations include diet, exercise, weight loss, alcohol abstinence, and "sleeping in a body position other than supine, keeping airway patent" (Barnes et al., 2009). The primary specific treatment for OSA is continuous, positive airway pressure (CPAP) (Barnes et al., 2009; Lopez-Jimenez et al., 2008). CPAP is not easily applied by all patients and has low adherence (Galetke et al., 2011; Kakkar & Berry, 2007). CPAP treatment must include education, adherence monitoring, early intervention for side effects, and telephone and clinic support for successful outcomes (Galetke et al., 2011). The research pursued here is intended to improve the accuracy and precision of airway assessments, possibly assisting current OSA treatment methods by providing quick, efficient, affordable and quantitative diagnoses and thus individualized treatments for patients.

Dental Treatment and Cephalometric Assessment

Conventional cephalometric analysis (CCA) involves the identification of anatomical landmarks and the recording of various measurements characterizing their spatial relationships including linear distances, angles, areas and linear ratios. These measurements are effective since quantitative standards can be achieved for age, gender, and pathology- based samples so that an individual can be compared statistically. The patient can also be compared to an earlier or later time point to quantitatively monitor treatment effects (Grauer et al., 2009). Sophisticated

multivariate statistical analyses such as principal component analysis (PCA) can be applied to provide multi-dimensional information. CCA is widely applied in dentistry and it exists as the standard method to assess skeletal relationships and spatial relationships resulting from treatment with orthodontic appliances (Grauer et al., 2009).

Current use of CCA to assess pharyngeal morphology includes clinical evaluation of airway obstruction of the face, mouth, nasal cavity and the pharynx (Togeiro et al., 2010). Oropharyngeal junctions have also been analyzed (Dalquivist, 2007; Mohsenin, 2001). Many studies involve measurements of airway length and anteroposterior and lateral distances of the airway (Abramson, Susarla et al., 2010; Walsh et al., 2008; Shigeta et al., 2008). Thus CCA is not only routinely used for dentistry, but CCA is also used to assess pharyngeal morphology.

CCA has significant limitations even though it enjoys widespread application. CCA is based on the subjective selection of anatomical landmarks that are considered to be important, but without biological justification necessarily (Bookstein, 1996). Quantitative measures represent biological structures directly between the anatomical landmarks selected for analysis, but surrounding tissue is not covered by those same measurements. Multivariate statistics can be vague and imprecise, since numerous dimensions must be simultaneously considered. Also, linear measurements do not account for overall size of the individual, and shape information is not explicitly identified through standard CCA. Thus, morphometric methods that can account for the entire airway anatomy is highly desirable (Lenza et al., 2010). The ability to express form difference as size and/or shape change would also prove useful since these parameters could infer very different biological meanings and provide a greater understanding of structures being assessed (Kranioti et al., 2009; Monteiro et al., 2002).

CCA is widely employed due to its inexpensive cost and ease of use (McIntyre & Mossey, 2003). However, new geometric morphometric analysis (GMA) tools are being developed for inexpensive and ease-of-use implementation. GMA, the quantitative study of biological shape variation is popularly used for medical imaging and anthropology (Bookstein et al., 2004). GMA attempts to quantitatively define both size and shape features of a biological structure (Lele & Richtsmeier, 1990) and it may identify landmarks that account for similarities and differences in

shape (Pavlinov & Mikeshina, 2002). GMA includes morphometric techniques including Procrustes superimposition (PS), Thin Plate Spline analysis (TPS), Euclidean Distance Matrix analysis and Finite Element Analysis (McIntyre & Mossey, 2003). PS and TPS are "the most powerful techniques in landmark-based morphometrics and may be combined for multivariate statistics and imaging" (Bookstein, 1997:225). PS uses a series of landmarks which are first scaled to the same size and then followed by rotation to achieve a minimum of positional variance at each landmark (Pavlinov & Mikeshina, 2002). The consensus, or mean configuration, and residual, or the variance around landmarks, is calculated and plotted. To test for significance between residuals, an F-test can be used to test for shape variance while TPS can be applied to map shape variance to the model (Lozanoff et al., 1994; Kristenson et al., 2008). In addition, TPS quantitatively analyzes shape deformations between two landmarked forms matched to have the smallest bending energy or shape change possible and is very useful in visualizing shape changes (Bookstein, 1997; McIntyre & Mossey, 2003). TPS results can be displayed by a transformation model that shows type, amount, and location of shape differences (Pavlinov & Mikeshina, 2002). Dense- correspondence analysis (DCA) utilizes TPS for local alignment and PS for overall alignment when comparing a source image to a target image to create a warped model showing how much the source varies from the target (Hutton et al., 2003; In Seol et al., 2009). Thus, GMA provides a dynamic comparison between shapes encompassing the entire 2D or 3D structure rather than simple linear measurements that only describe limited 2D relationships.

Cone Beam Computed Tomography and Imaging

Cone Beam Computed Tomography (CBCT) was developed for patient assessment within the dental office (Gray, 2010). CBCT is a form of computed tomography that uses a conical-shaped X-ray beam to provide sequential 2D axial images, and reduces scanning time and radiation exposure while increasing accessibility compared to standard CT or MRI methods (Gray, 2010). Two-dimensional images are digitally recorded in a "Digital imaging and communications in medicine" (DICOM) format which was adopted as an industry standard in

1993 (DICOM, 2008). Although standard CT imaging provides numerous advantages, such as metal implant visualization, identification of the periodontal ligament space, enamel-dentin interface imaging, and dental root visualization, CBCT provides excellent images and its slight visualization disadvantages are outweighed by its efficiency, availability and ease of access (Holberg et al., 2005). CBCT became widespread in dentistry for multiple purposes, including surgical planning, orthodontics, and endodontics, due to CBCT's ability to create images which capture real anatomic sizes and shapes (Grauer et al., 2009; Chenin, 2010). Measurements from CBCT scans are closer to physical measurements than those from 2D slices and 2D projection images, and CBCT scans give rise to highly accurate 3D CBCT constructed models, which remain accurate even with small variations in patients' head positions (Hassan et al., 2009). CBCT may also be acquired and compared among different time points to analyze cephalometric changes due to growth, treatment, and aging (Grauer et al., 2009). Among examiners, identification of landmarks on CBCT scans is consistent in location and preciseness (Schlicher et al., 2011). CBCT continues to have widespread applicability and great accuracy in dentistry.

The widespread applicability of CBCT technology recently includes quantitative description of the upper airway in research attempting to quantify the airway (Osorio et al., 2008; Tso et al., 2009). From CBCT digital reconstruction, the aboral region of the oropharynx displayed the most constriction in the pharynx (Tso et al., 2009). Also, participants had concave, round, or square shaped airways (Ogawa et al., 2007). CBCT could provide a useful approach for non-invasively assessing the airway and identifying any morphological abnormalities. Even soft and hard tissue, such as the tongue and mandible, in relation to the airway can be assessed in 3D reconstructions of the airway derived from DICOMs obtained through CBCT (Ogawa et al., 2007; Cevidanes et al., 2006). Since CBCT 3D imaging improves airway evaluation, especially at sites of obstruction (Grauer et al., 2009), CBCT 3D images have the potential to become an industry standard, but further research is necessary to validate this assertion. Regardless, analytical software that automatically identifies airway boundaries and captures specific airway morphology remains imprecise and time-consuming. Also, there is little information available showing whether these models can be used to detect specific morphological features of the entire upper

airway. Few studies include the nasopharynx (NP) in 3D airway models and further studies of the airway are necessary (Grauer et al., 2009).

Airway3D Software

CBCT appears to provide an important method for fast, reliable and inexpensive imaging of the airway; however, the ease-of-use system for generating airway models and quantifying pharyngeal architecture using an objective, straightforward approach remains problematic. Currently, there are at least 27 programs designed for viewing DICOMs, many of which have imaging capabilities (Molen, 2011). Popularly used 3d imaging programs include 3dMDvultus software (edMD, Atlanta, GA), Dolphin Imaging (Dolphin Imaging, Chatsworth, CA), and InVivoDental (Anatomage, San Jose, CA) (Grauer et al., 2009). These programs include common features including airway segmentation with 3D model construction and highlighted DICOMs, threshold segmentation, smoothing filters, exporting models, and the ability to calculate airway volume and surface area (Grauer et al., 2009). Dolphin3D, InVivoDental, OnDemand3D (CyberMed, Seoul, Korea), and OrthoSegment (Case Western Reserve University, Cleveland, Ohio) have been shown to have good reliability, but low accuracy in constructing 3D models from manual airway identification and determining airway volume (El & Palomo, 2010). Automatic airway segmentation was shown to have clinically insignificant differences to manual segmentation while having the benefit of greatly reducing procedure time (Shi et al., 2006).

Recently a software program named Airway3D was developed for imaging, using automatic airway extraction techniques, and quantitative assessment of the airway for both size and shape variables (Celenk et al., 2010). Although Airway3D does not include airway cross-sectional calculations of 3dMDvultus software, or combining CBCT with a 2D photograph of Dolphin Imaging, Airway3D constructs, exports, and imports 3D models of airway, soft tissue, and hard tissue (Farrell, 2009). This method takes advantage of graphics processing unit (GPU) approaches utilizing computing unified- device architecture, CUDA, by NVIDIA (Noel et al., 2009) to greatly increase speed of model generation and imaging. Compared to CPU, data has showed that computation time was close to 28 times faster utilizing CUDA on the GPU (Farrell, 2009).

Other features of the Airway3D system includes 2D CBCT image slices or DICOM loading and 3D Gaussian Filter (GF) smoothing of those slices for continuous airway boundary identification, followed by airway boundary- extraction. The boundary- extraction method has been improved so that the airway in CBCT scans can automatically be identified and outlined, and a model can be generated in less than one second, providing for real- time assessment. Another feature is threshold segmentation, which is used to find consistent pixel characteristics in CBCT scans being used for airway model rendering. Threshold segmentation allows for accurate separation of bone or airway from soft tissue and background (Hassan et al., 2010). Extraction, segmentation, and reconstruction of bone and other air volumes of interest are also available. Airway3D also exports and imports 3D anatomic models, combines these models with CBCT slice images, so that models may be edited to exclude extraneous surface volume or smooth surface volume. Airway differences may be both qualitatively and quantitatively identified by utilizing CCA, PCA, PS, and DCA. Dense correspondence combines the powerful tools of PS and TPS to warp a 3D airway model to a target model in order to locate and quantify both size and shape differences between those airways.

In summary, existing airway modeling software programs have distinct features that are combined in Airway3D. Airway3D not only dramatically expedites the assessment process while removing operator bias in order to insure accuracy and precision, but also performs traditional CCA and innovative DCA to compare airway size and shape variables independently.

Specific Aims

Advances in 3D imaging of the airway appear to provide diagnostic advantages since quantitative measurements can be easily and accurately applied for objective classification and characterization of the pharynx. However, a CCA approach is likely to miss important features since CCA does not consider the entire detailed morphology, which is characteristic of the pharynx. Thus, recent advances by investigators have attempted to partition CCA into size and shape independent values (Abramson et al., 2009; Ogawa et al., 2007; Tso, 2009; Walsh et al., 2008). GMA approaches, such as TPS, successfully partitions overall morphology into size and

shape parameters, and along with PS alignment (Bookstein, 1997), GMA, including PS and DCA, may offer a much more effective method to quantify airway morphology. The purpose of this study is to validate computerized 3D models and the methods utilized to construct these models and to compare them. The overall objectives to be tested in this study is that computerized 3D models of the human- airway can be generated automatically from CBCT scans and that these can models can be compared and decomposed into quantitative and independent measurements of size and shape. The rationale for these objectives is that Airway3D software can be utilized effectively quantifying airway size and shape. If so, then the software can be applied to patients for the purpose of improving diagnosis and treatment of pharyngeal diseases.

Specific Aim 1 is to assess the usability of Airway3D's airway extraction methods. This includes assessing automatic airway boundary- extraction, GF effects, and threshold efficiency. The rationale for this aim is to determine whether the airway can be extracted effectively so that subsequent modeling methods can be performed effectively.

Specific Aim 2 is to assess the accuracy of model rendering of patient airways and landmark identification and reliability. The rationale of this aim is to determine whether TPS and other GMA methods can be applied to airway models to assess and quantify airway size and shape separately.

Specific Aim 3 is to implement the Software to compare male and female airways to determine whether meaningful GMA data can be generated with Airway3D. The rationale of this aim is to determine whether gender differences exist. It is expected that male airways will be larger in size than female airways, but size-independent shape values would not differ between genders.

Results of this study should demonstrate that detailed 3D modeling of male and female airways can be performed, and 3D models can be compared morphologically using both size and shape-only measures using the features of Airway3D technology.

CHAPTER 2. MATERIALS AND METHODS

Design

This is a retrospective study analyzing the male and female pharynxes from anonymous CBCT DICOMs from an existing database. The design included three steps. First, the usability of airway boundary- extraction methods from male and female CBCT, including Gaussian filter and threshold efficiency, was assessed, followed by an assessment of the accuracy and reliability of model rendering and landmark identification. Lastly, Airway3D software was used to compare male and female airways to determine if male and female airway morphometric differences existed as expected.

Subjects

Twenty subjects' DICOMs were anonymized and randomly selected from a pre-existing database housed at the Creighton University School of Dentistry through Dr. Neil Norton. Dr. Norton routinely collects CBCT scans from adult patients in the Creighton Dental Clinic in Omaha, Nebraska. The subjects were single-blinded randomized into groups based on gender. Upper airway scans were collected following the standard HIPAA regulations for use in research under his current and active IRB proposal (IRB #10-15790). CBCT scans were taken by the Creighton Dental Clinic using the I-ICAT machine made by Imaging Systems. Patients sat upright and scans were collected per patient with a slice thickness of 0.3 mm at 1024 x 1024 resolution. Scanning time was 20 seconds. CBCT images were saved at approximately 300 DICOM files per patient. This study is classified as exempt through the University of Hawaii Institutional Review Board (CHS #18841).

Procedure

Specific Aim 1. Airway Extraction

To assess airway boundary- extraction methods, each participant's DICOM or CBCT slices were loaded into Airway3D and evaluated using sagittal, transverse, and coronal CBCT image views to confirm airway patency and DICOMs included the pharynx from the most superior border of the NP to the base of the epiglottis (EB)**.** Airway3D performed automatic boundary-extraction to outline the airway along the soft tissue surrounding the pharynx. PCA axes identified the center axis of the airway, which allowed for quick identification of the airway, shown in Figure 1 (Farrell, 2009). Thus, placement of white outlines on soft tissues surrounding the airway should be quick, and include the entire airway.

The automatic airway segmentation, or construction of 3D virtual surface models (Grauer et al., 2009), identifies black colored pixels as airway, and grey and white colored pixels as soft tissue, allowing for automatic identification of pharyngeal walls (Farrell, 2009) in place of manual outlining of the airway in each DICOM slice, which is both time consuming and not clinically feasible (El & Palomo, 2010; Shi et al., 2006). Since the pharynx is continuous with nasal and oral cavities, trachea, and esophagus, user-defined airway borders included EB and most posterior points of the more anteriorly located right or left inferior nasal conchae (INC). User-defined oropharynx borders which included hard palate (HP) and tip of the epiglottis (ET) or EB shown in Figure 2.

Threshold alterations were performed to define the appropriate shade of pixels, based on a grey scale, which allowed for the most distinction between the dark airway and surrounding soft tissues. The pixel grey scale is from 0 to 256, with 0 having no light, for a color of black on CBCT scans, and 256 having maximum light, for a color of white on CBCT scans (Farrell, 2009). Thus, moving from threshold levels 0 to 256, increasingly lighter shades of black pixels were included in airway segmentation, which simultaneously increased airway model volume (Figure 3). Threshold values for each participant were sequentially modified in increments of five, from one to 80, and automatic airway segmentation constructed 3D airway models of NP to EB, at each threshold

increment with GF level 3. The threshold value that increased airway model volume the least, from the previous threshold value's airway volume, was selected to create individualized patients' representative airway models.

GF creates smoothed CBCT images and airway models by blurring each CBCT slice to create a continuous boundary between the airway and soft tissues, which was shown to be more representative of the airway (Figure 4) by reducing image noise (Sagawa, Miyoseta, Hayakawa, & Honda, 2009). GF will be assessed by randomly selecting a male and female CBCT images, reconstructing airway models at ideal threshold and increasing GF levels 1 through 10 in increments of two, and by comparing any changes in airway models. With increasing GF level, airway models are expected to visually appear similar, with airway model volume and surface area expected to remain consistent.

Specific Aim 2. 3D Model Accuracy and Landmark Reliability

Representative individual 3D airway models were constructed using Airway3D's automatic airway segmentation. Airway segmentation at GF level three with patient-specific threshold values, should allow for low background interference from CBCT scans and definition between soft tissue and the airway. Three models of the airway to be segmented are of NP to EB, HP to ET and HP to EB. Airway models were qualitatively assessed for inclusion of the complete defined airway and exclusion of soft tissue and sinuses by referring to the airway model itself and by highlighting airway regions within each selected CBCT slice used to reconstruct the airway model.

To validate three airway models, they were assessed for validity of volume and surface area measurements by comparing them to previous studies. NP to EB airway models were used in both GMA and CCA analyses. Airway models were also assessed qualitatively for accuracy by identification of expected features on all airway models. Identifiable features of the airway model NP to EB included lateral pharyngeal recesses, auditory tubes, uvula, choanae, torus tubarii, valleculae, glossoepiglottic folds, ET, most posterior points of both right and left INC and meatus.

Because locating landmarks on CBCT slices have been reported to be more accurate than identifying landmarks on rendered models (Grauer et al., 2009), landmarks listed in Table 1 were identified for each airway model of NP to EB by manual identification on each participant's CBCT DICOMs (Figure 5). To test for user reliability, landmark identification was repeated five times for four randomly selected female patients and four randomly selected male patients. Each trial was completed at least one hour after the previous trial. PS combined each series of landmarks to visualize variances of each landmark and to quantify these variances for repeated male and female series. Average male and average female landmark variations were generated using PS. To test for reliability, Procrustes models were scaled removing size differences, and residuals were automatically calculated and compared between the replicates and averages of male and female groups. An F-test was used to compare replicate male and female landmark variances to male and female average landmark variances for significance. Differences within male or female replicates are expected to be significantly less than between demonstrating good user reliability for identification of landmarks on CBCT DICOMs.

Specific Aim 3. Geometric Morphometric Analyses

Male and female models were compared utilizing parameters of size and shape. Airway models' comparisons of size included airway volume, areas, and linear measurements, summarized in Table 2. Six linear measurements were chosen that most closely identify airway length, anteroposterior, and lateral distances between previously identified landmarks. Male and female airway volumes and surface areas and linear measurements within and between subjects were compared with one-way analysis of variance (ANOVA) using the IBM Statistical Package for the Social Sciences (SPSS) Statistics 19.0, which was expected to show that differences exist between average male and female airways.

To assess the reliability of six linear measurements based on manual landmark identification, intra-class correlation (ICC), or ratio of between-participant variance, and SEM, or consistency/precision of scores of individuals (Weir, 2005), tests were performed for each replicate male and female measurement. SPSS and Microsoft Excel were used to calculate ICC

and SEM values. ICC is typically used; however since it is based on between-subjects differences, SEM, which is based on within-subjects differences, was also calculated. ICC of 1.0 shows scores are without error and are 100% due to true score variance, and a small SEM means greater reliability in identifying individuals' true scores (Weir, 2005). Also, PCA plots assessing six linear measurements of replicate male and replicate female models were expected to show very tight clustering of replicate models, meaning very little variation in user-defined landmarks. Because linear measurements were based on selected distances between manually identified landmarks, little variation in PCA and high ICC would support both Specific Aim 2 and 3, by linear measurement reliability and user reliability in digitization.

When comparing male and female linear measurements, PCA was expected to separate male and female participants into two clusters, and to find both size and shape variation in linear measurements between males and females. Size variation was indicated by PCA axis 1 while shape information was expected to be shown by five following PCA axes. The linear measurements that account for the most size and shape variation were used for DCA validation.

Airway shape was also analyzed by GMA techniques PS and DCA. For PS, all scaled and unscaled landmark models were compared using F tests. Significant F-tests were expected to quantify differences in size or shape of male and female landmark models but not identify where these differences were located on airway models.

DCA utilizes PS to match landmark models for overall alignment and TPS to quantify airway model size and shape differences and to create local alignment of a source image to a target image. Because CCA and PS analyses resulted in significant differences in both size and shape, DCA was expected to identify and to quantify possible airway gender differences by colored warped models for location of deformations, or 'hot spots', and color scale bars to quantify areas by their largest deformations. First, to assess DCA functionality, a female landmarked airway model was warped, or fitted, into itself for shape. We expected no deformation in the colored warped- initial model, to show that DCA conforms to expectations.

Next, an initial model was warped to fit a target model for size, then for shape. All models, excluding Male 9, were randomly selected without replacement, for nine size and nine

shape comparisons. For size analyses, a female landmarked airway model was warped to a male unscaled landmarked airway model, to create a colored, quantified warped- initial model, and repeated for a total of nine comparisons. This was repeated with scaled models for shape analyses. All deformations, shown in purple and red on the colored warped- initial model, were expected to be few in number, quantitatively small, and spatially consistent, and isolated, to show that DCA is effective and results are interpretable. DCA was expected to show increased specificity in locating size and shape differences between airway models by identifying viable 'hot spots' not only at landmarks, but between landmarks. Lastly, locations of any size and shape 'hot spots within a single comparison are expected to differ, showing possible separation of size and shape analyses.

To validate DCA in identification and quantification of gender differences in size and shape, deformations were compared to results of PCA. 'Hot spots' were compared to PCA results; large linear measurement size and shape variations were expected to correspond spatially and quantitatively with 'hot spots' on airway models. This would suggest that DCA results are valid, and that DCA may be a new GMA method to successfully separate size and shape parameters for the pharynx.

CHAPTER 3. RESULTS

Specific Aim 1. Airway Extraction

Automatic boundary- extraction quickly outlined the NP to EB, and for five out of twenty participants, boundaries were manually adjusted to include the entire airway and exclude non-pharyngeal structures, e.g., sphenoidal and maxillary sinuses. Manual boundaries were quickly and easily defined for each participant.

To determine individualized, representative threshold levels, Airway3D automatically computed airway segmented volumes based on selected threshold values that were arbitrarily selected between grey scale values of 5 to 80. Representative thresholds were chosen where segmented volumes graph plateau (Figure 6), suggesting that volumes stabilized over this grey scale interval. This interval represented the optimal threshold that maximizes airway space while minimizing soft tissue regions, to effectively separate the airway from pharyngeal walls. Threshold values ranged from 25 to 55, which was 11.7% of possible threshold levels 0 to 256. The average optimal threshold level was 40 for both male and female participants.

To assess GF, randomly selected female and male DICOMs were segmented at optimal threshold and GF levels 2 through 10. From GF 2 through 10, female 7 airway volume increased from 13,713.5 mm^3 to 13,994.8 mm^3, a 1% change, and male 1 airway volume increased from 26,812.4 mm^3 to 27,211.1 mm^3, a 1% change. With increasing GF, Female 7 airway model surface area decreased from 6445.17 mm^2 to 6264.94 mm^2 and male 1 airway model surface area decreased from 9651.26 mm^2 to 9527.86 mm^2. With increasing GF level, all expected features of 3D models remained. CBCT transverse and sagittal views of female 7 and male 1 with GF 2 and GF 10 applied to scans displayed increased smoothing of DICOMs and 3D airway models with higher GF level Figure 7. As GF increased, CBCT scans were increasingly

smoothed, so PCA axes, that identified the middle of the airway, became increasingly straight or linearized.

Specific Aim 2. 3D Model Accuracy and Landmark Reliability

Figure 8 displays examples of airway models at optimal threshold and GF level 3. All expected identifiable features were found on airway models. Features included uvula, glossoepiglottic fold, epiglottic, and INC indentations, torus tubarii, auditory tubes, valleculae, lateral pharyngeal recesses, and choanae. All airway models displayed landmark features, included relevant airway regions, and excluded sphenoidal and maxillary sinuses and oral cavity.

As a test for user landmark identification reliability, replicate PS models for Female 1, 2, 7, and 9 and Male 1, 2, 5, and 10 were compared to group average PS models for females and males. Landmark variances were visually smaller within patients than between patients (Figure 9). Residuals were calculated (Figure 10) and compared between the average iterative model (within model variation) versus the average Procrustes models generated from the group samples of males and females (between model variation), respectively (Figure 11). Results show that variation between Procrustes landmark configuration is significantly greater than within variation (Table 3).

Specific Aim 3. Geometric Morphometric Analyses

Preliminary data presented Male 9 DICOMs to have an airway volume of NP to EB (AV) of 9,937 mm^3, compared to the average male AV of 27,305 mm^3. PCA of linear measurements also showed small values for Male 9 (Figure 12), and PCA plots, of axes 1 to 2 and 1 to 3, placed Male 9 separately from the group of male participants (Figure 13). Male 9 appeared to be an outlier and was excluded from both CCA and GMA.

For CCA results for size analyses (Table 4), Male AV waw larger than female AV at all threshold levels (Figure 14), but results were not significant at individual threshold levels. Average female and male airway volumes at representative threshold are graphed in Figure 15 showing that male airway volume was larger than female airway volume in all three models, but

significantly larger from HP to EB (OVB), $F(1,17) = 5.495$, $p < .05$, and HP to ET (OVA), $F(1,17) = 4.507$, $p < .05$. Male surface area of model from HP to EB (SAB) was significantly larger than female SAB, $F(1,17) = .04$, $p < .05$. Significant differences were also found for LA $F(1,17) = 7.794$, $p < .05$, Male LB $F(1,17) = 11.024$, $p < .01$, and APB $F(1,17) = 4.872$, $p < .05$.

For linear measurement and manual landmark identification reliability, ICC results (Table 5) show measurements are reliable and accurate to a very high degree. PCA for linear measurements LA, LB, LATA, LATB, APA, and APB compared replicate landmark models of female 7 and male 1. PCA table (Figure 16) showed largest amount of variation in PCA axis 1. PCA 1 accounted for 99.6% of total variation. PCA plot of PCA 1 by 2 (Figure 17) displayed very distinct groups of female 7 and male 1 replicates along PCA 1.

PCA comparing female and male groups resulted in 59.34% of total variation explained by PCA 1 as size variation and 18.93% by PCA 2 and 12.4% by PCA 3 as shape variation listed under lambda of Figure 18. Most of size variation was captured by measurements LA and LB of PCA1, and most shape variation was shown by LatA, ApA, and ApB of PCA 2 and 3. Measurement specific variations were quantified under loadings of Figure 18. PCA Plot of PCA 1 by 2 and 3 (Figure 19) showed clustering and slight overlap of females and males along PCA 1.

For GMA, female and male landmark PS model (Figure 20) F test analysis (Figure 21) calculated significant F values for size and shape (Table 6). DCA of the female base model imposed upon itself, created a mostly blue and green colored warped- initial model, representing no size or shape differences. For DCA warping individual females to fit individual males for size and then shape, all warped- initial models displayed few, isolated, and quantified hot spots located at and between landmarks, and all expected features were on warped- initial models. (Figure 22 and Table 7). Average size deformation was 15.05 ±6.50 mm^3 located variably among warped-initial models at landmarks 1 and 2 positioned at the superior aspect of the model; 5, 6, 7 and 8 at the inferior aspect of the model, and 13, 18, and 21 at the oropharynx. Deformations were also found between landmarks at lateral pharyngeal recesses, the oropharynx, and the superior and inferior aspects of airway models. Average shape deformation was 0.10 ±0.04 mm^3 located erratically at landmarks 6, 13, 18, and 21. Shape deformations were also found at lateral

pharyngeal recesses, anterior oropharynx, and posterior aspect of airway models.

CHAPTER 4. DISCUSSION

Specific Aim 1. Airway Extraction

Automatic airway boundary detection was quick and efficient, and optimal threshold range was small for both females and males, showing practicality and possible clinical usage of airway boundary- extraction and thresholding for airway segmentation. Increasing GF smoothing did not significantly alter airway model morphology, and airway volume and surface area remained qualitatively consistent of 1% changes in volume and surface area with increasing GF. Fluctuating increases in airway volume and decreases in surface area may be due to the boundaries of the airway becoming increasingly smoothed for more pixels to be included into airway segmentation, resulting in less coarse 3D airway surface models and possibly increasing airway volume (due to more pixels) and decreasing airway surface area (due to less ridges) of airway model. These results were consistent with previous studies, where GF was useful in reducing background noise with minimal morphological changes (Sagawa et al., 2009; Farrell, 2009). These findings indicate that Airway3D can quickly and effectively perform airway extraction techniques for building 3D airway models.

Specific Aim 2. 3D Model Accuracy and Landmark Reliability

Average AV was similar to findings of Tso et al. (2009), OVB to Abramson et al. (2009), and OVA to Shigeta et al. (2008, 2011), Ogawa et al. (2007), and El and Palomo (2010). SA was also consistent with Abramson et al. (2009). These results show that Airway3D volume and surface area measurements are analogous to previous studies using various imaging programs. Along with displaying numerous identifiable airway features, valid 3D airway models demonstrate that Airway 3D can successfully perform airway extraction and automatic airway segmentation. Airway models generated with Airway3D also included a larger number of identifiable features and greater detail than previous studies and programs, including Amira, OsiriX, Mimics 9.0

Materialise, CBWorks, Dolphin3D, InVivoDental, On Demand3D, and OrthoSegment, used to reconstruct the upper airway, creating 3D models (Ogawa et al., 2007; Osorio et al., 2008; Vos et al., 2007; Tso et al., 2009; El & Palomo, 2010; Shigeta et al., 2011).

Results show that variation between PS landmark configurations is significantly greater than within variation, reflecting a high degree of accuracy for digitization directly on CBCT slices. 3D airway models are accurate and manual landmark identification is reliable, thus GMA methods may be applied to analyze and to quantify airway size and shape parameters separately.

Specific Aim 3. Geometric Morphometric Analyses

For CCA, Male AV is not significantly larger than female AV, supporting previous studies (Abramson et al., 2009; Shigeta et al., 2011). Male and female AV not having a significant difference is most likely due to pharyngeal morphology that includes many folds characteristic of the pharynx, e.g., the variable lateral pharyngeal recesses. Significant differences in OVA, OVB, and SAB were found in this present study, contradicting findings of Abramson et al. (2009) who reported no significant differences in gender for airway volume and surface area. Linear measurements and significant gender differences in LA, LB, and ApB were also consistent with previous studies (Susarla et al., 2010; Abramson et al., 2009; Sawani et al., 2010). Our findings disagreed with those of Abramson et al. (2009), stating no gender differences in airway length, but results from the current student corresponded with those of Susarla et al. (2010) stating gender differences in airway length exist. These contradictory findings may be attributed to the number of subjects in this study compare with Susarla et al. (2010) the included more subjects (20 and 32 participants respectively). However, CCA results were generally consistent with the literature suggesting that Airway3D can effectively perform CCA of the upper airway.

Intraclass correlation analysis resulted in ICC's for each individual measurement set above 0.993. Overall ICC for all repeated measurements was greater than 0.999. Though there is no established ICC value for evaluating reliability (38), when viewed with the overall standard error of the mean (SEM), calculated in this case to be 0.09 cm for all measurements, an ICC above 0.999 seems to indicate a considerably high level of measurement reliability in the present

study. ICC results display reliable measurements comparable to previous studies (Abramson et al., 2009). Because linear measurements are based on manual selection of landmarks, digitization on CBCT images remained an accurate technique, agreeing with previous studies (Grauer et al., 2010; Schlicher et al., 2011). PCA of replicate landmark models showed distinct clustering of models almost entirely for size, meaning very little variation in linear measurements and, indirectly, manually identified landmarks. Thus ICC and PCA display that there is very little variation in linear measurements, for strong reliability in landmarks.

PS quantitatively affirmed that significant size and shape differences between female and male airways do exist, without identifying specifically where those differences are located. DCA can be used to warp one airway model into another identifying and to quantifying spatially consistent deformation found at and between landmarks. Most deformation was found at the lateral pharyngeal recesses and the nearby superior aspect of NP. Some deformation was also found at the oropharynx, which is consistent with literature finding that OSA patients have most restricted airways at the oropharynx (Tso et al, 2009; Shigeta et al, 2011). Further investigation is necessary to determine if this deformation at the oropharynx is consistently due to gender or disease states. Variation of size and shape of the lateral pharyngeal recesses may be due to pharyngeal wall mucosa compressing , which is shown to be alleviated in only 83% of subjects when CBCT is performed with patients sitting upright (Sutthiprapaporn et al., 2008). Lateral pharyngeal recesses have also been shown to be asymmetrical (Sutthiprapaporn et al., 2008), which may further contribute to variation in size and shape of the lateral pharyngeal recesses. DCA of size and shape for airway models of HP to ET or EB may locate additional areas of deformation. Size ‘hot spots were located mostly at the superior and inferior aspects of warped airway models, and shape ‘hot spots’ were mostly at the middle of the warped airway model. Size and shape ‘hot spot’ locations within comparisons differed, and in 4 out of 9 comparisons, size and shape ‘hot spot’ locations were the same. These results suggest that both size and shape differences do exist between males and females, DCA can be performed, and DCA can separate size and shape variation.

To validate DCA, DCA results were compared to PCA findings. PCA identified areas of largest variance as measures LA and LB, and both measurements were consistent with DCA analyses identifying largest size distortions at the most superior and inferior aspects of warped-initial models. PCA found areas of largest shape variance as measures APA and APB and DCA shape analyses located largest 'hot spots' in the region of the uvula and lateral pharyngeal recesses, which also fall along measures APA (landmark 3 to 28), and APB, (landmark 13 to 18). Furthermore, PCA also quantified individual linear measurements. Differences between male and female linear measurements of largest variation for size, LA and LB, corresponded to DCA quantification of deformation. Increasing DCA size values corresponded with increasing differences between linear measurements. Use of DCA allowed for localization and quantification of both size and shape differences located at landmarks and between landmarks, which is consistent with, and more specific than, established PS and PCA measures. Size 'hot spot' quantification is valid, and further analysis of shape quantification, using other methods, is necessary. Overall, it appears that linear measurements and volumes cannot adequately describe the airway (Lenza et al., 2010) and DCA provides a novel approach for separating and quantifying airway model size and shape.

There are limitations to the current study. Limitations include a small sample size and landmark identification. First, many studies find both significant and non-significant differences between male and female airway volumes and linear measurements (Abramson et al., 2009, Sawani et al., 2010, Susarla et al., 2010). A larger sample size should not only provide increased validity for Airway3D's airway extraction, airway segmentation, and CCA and DCA techniques, but might provide for standardization of airway size and shape parameters from CBCT DICOMs.

Secondly, selected landmarks do not necessarily need biological significance, but landmarks remain the gold standard for CCA comparing males and females, or normal to disease states (McIntyre and Mossey, 2003). This study focuses on validating the usage of landmarks for DCA overall alignment, not necessarily for the actual biological significance of landmarks.

Lastly, the gold standard ICC, and rarely the less known SEM (Weir, 2005), has been used in few studies to validate the reliability digitization of these selected landmarks on CBCT

(Abramson et al., 2010; Moshiri et al., 2007) and some use less effective correlation statistics (Grauer et al., 2010). The methods used in this present study to calculate ICC and SEM are based on selected linear measurements between these manually identified landmarks. Thus, ICC is more representative of the reliability of measurement between two landmarks, than individual landmark reliability. It is not possible to determine the variability of one or both landmarks of a measurement using ICC. This study attempted to solve this by use of PS to compare shape variability of individual landmarks within patients to shape variability of individual landmarks between patients. Because variability between patients can be very large, this could easily mask considerable differences in replicated landmark locations when compared using PS. Large differences in one replicated landmark location may also affect shape variation used in PS. It seems that another mathematical function is needed to compare variability within each landmark to validate landmark identification reliability.

CHAPTER 5. CONCLUSIONS AND FUTURE WORK

The purpose of this study, to implement and validate Airway3D for quantifying pharyngeal size and shape, was successfully achieved. In support of the objectives, the present study demonstrates that computerized 3D models of the human upper airway can be generated automatically from CBCT DICOMs, and that these 3D models can be compared and decomposed into quantitative and independent measures of size and shape using novel DCA analyses of Airway3D, validated by established CCA, PS, and PCA analyses. This present study provides insight into GMA of 3D models through DCA. Airway3D is the first program to develop DCA and to successfully quantify and separate size and shape of 3D airway models.

Airway3D has multiple possible commercial uses. It quickly and efficiently constructs valid, detailed 3D models, possibly making it the new modeling program of choice for the clinic or for research. It has the ability to perform and quantify CCA analyses commonly used in dentistry, orthodontics, endodontics, and surgery (Grauer et al., 2009; Chenin, 2010) and may have the ability to compete with currently available software, which could be further supported with completion of comparison studies. With available software of Airway3D, it could perhaps be validated in the clinical setting, such as comparing a patient's pre- and post-operative anatomy.

Future work includes continuing to assess the accuracy of Airway3D's models; models of the present study could not be compared to skeletal, cadaveric, or silicone models. In addition, because DCA of Airway3D located shape hot spots not identifiable through previous PS and PCA results, this present study demonstrated that DCA is possible, but further analysis to assess if these hot spots are correctly located, is necessary. This may be achieved by comparing one airway model to itself on various size- scales, or by altering one aspect of an airway model and comparing the initial model to altered model.

Lastly, the novel Airway3D DCA is being developed to warp multiple airway models at a time; this is expected to assist with identifying specific localization and quantification of size and

shape deformations between a single diseased model and an average of normal male or female model. This function may not only have the ability to assess and quantify average normal and diseased upper airway models, but it may assist with the imprecise diagnosis and treatment of diseases like OSA.

APPENDIX A. TABLES

Table 1. Anatomical Landmarks for Airway Model of Nasopharynx to EB

Landmark Number	Description
1	Most superior point on left posterior choanae
2	Most superior point on right posterior choanae
3	Medial most point on right torus tubarius
4	Medial most point on left torus tubarius
5	Most anterior point on left valleculae
6	Most anterior point on right valleculae
7	Lateral most point on right lateral glossoepiglottic fold
8	Lateral most point on left lateral glossoepiglottic fold
10	Most superior point on vomer
13	Posterior point on airway opposite the anterior most point of C1 arch
18	Posterior most point of uvula
21	Posterior point on airway opposite the anterior most point of C2 body
26	Posterior most point on left inferior concha
28	Posterior most point on right inferior concha

Table 2. Definitions for Size Airway Parameters

Measurement	Symbol	Description
Airway Volume	AV	Volume of airway from nasopharynx to the base of epiglottis
Oropharynx Volume A	OVA	Volume of airway from hard palate to the tip of the epiglottis
Oropharynx Volume B	OVB	Volume of airway from hard palate to the base of the epiglottis
Surface Area of Airway	SA	Surface area of AV
Surface Area of Oropharynx A	SAA	Surface area of OVA
Surface Area of Oropharynx B	SAB	Surface area of OVB
Length A	LA	Distance between most posterior point on right inferior choanae and most anterior point on right valleculae (Landmark 2 to 6)
Length B	LB	Distance between most superior point of vomer and posterior most point of uvula (Landmark 10 to 18)
Lateral Distance A	LATA	Distance between medial most point of right and left torus tubarius (Landmark 3 to 4)
Lateral Distance B	LATB	Distance between lateral most points on right and left lateral epiglottic folds (Landmark 7 to 8)
Anteroposterior Distance A	APA	Distance between medial most point of right torus tubarius and posterior most point on right inferior concha (Landmark 3 to 28)
Anteroposterior Distance B	APB	Distance between posterior most point on the airway opposite the anterior most point on C1 arch to posterior most point of uvula (Landmark 13 to18)

Table 3. Scaled, shape residuals for replicates and groups of females and males

Participants	**Residuals**	***F* value***	***p* value***
Replicates			
Female 1	.00126	436876	< .001
Female 2	.00151	335000	< .001
Female 7	.00201	917674	< .001
Female 9	.00148	530631	< .001
Male 1	.00104	419276	< .001
Male 2	.00177	662261	< .001
Male 5	.00207	997145	< .001
Male 10	.00101	436428	< .001
Group			
Females	.1599		
Males	.1383		

**F* values and *p* values represent replicate residual compared to group residual.

Table 4. Airway Size Parameters

	Male		Female		
Measurement	**Mean**	**SD**	**Mean**	**SD**	***p* value**
AV	27305.44	±4854.28	22354.51	±6953.51	>.05
OVA	15674.22	±2669	12207.05	±4187.05	<.05
OVB	20482.93	±4116.14	15777.27	±4581.95	<.05
SA	20605.14	±33728.13	8709.42	±1859.42	>.05
SAA	5478.9	±867.92	4899	±1222.2	>.05
SAB	7851.65	±1048.95	6554.24	±1439.02	<.05
LA	87.26	±6.44	77.49	±8.53	<.05
LB	83.63	±5.93	72.76	±8.04	<.01
LATA	17.95	±6.58	18.67	±4.10	>.05
LATB	17.64	±3.14	15.13	±3.27	>.05
APA	39.32	±6.51	36.61	±4.44	>.05
APB	27.90	±5.21	22.01	±6.29	<.05

Table 5. CCA Intra-examiner Variability

Measurement	Mean ± SD*	ICC(3,1)	SEM
LA	80.10 ± 10.80	0.998	0.422
LB	76.07 ± 10.00	0.999	0.371
LatA	18.22 ± 4.83	0.988	0.527
LatB	17.44 ± 3.80	0.992	0.347
APA	39.32 ± 6.17	0.992	0.540
APB	26.88 ± 5.66	0.998	0.276
Overall	43.01 ± 26.91	0.9997	0.444

*SD, standard deviation.

Table 6. Size and shape residuals for females and males

Parameter	Female	Male	*F* value	*p* value
Size	11724.3	7990.18	7.33711	< .05
Shape	0.15986	0.096722	563745	< .001

Table 7. DCA for Size and Shape

Size Analysis	Deformation	Location at Landmark	Other Locations
Female 1 to Male 7	18.1004	21	lateral pharyngeal recesses superior and inferior airway
Female 2 to Male 5	15.5012	1, 2	Lateral pharyngeal recesses superior airway
Female 3 to Male 8	13.0077	13	oropharynx
Female 5 to Male 1	11.1542	6, 7, 4, 8	oropharynx
Female 6 to Male 10	8.51728	4, 5, 18	superior airway
Female 7 to Male 6	28.0836	5, 6, 7, 8	lateral pharyngeal recesses inferior airway
Female 8 to Male 2	8.17055	5, 6, 28	lateral pharyngeal recesses inferior and posterior airway
Female 9 to Male 4	11.6992	18	N/A*
Female 10 to Male 3	21.2468	21	superior airway

Shape Analysis	Deformation	Location at Landmark	Other Locations
Female 1 to Male 7	0.144869	21	lateral pharyngeal recesses
Female 2 to Male 5	0.120133	21	lateral pharyngeal recesses superior and posterior airway
Female 3 to Male 8	0.101067	13	lateral pharyngeal recesses
Female 5 to Male 1	0.0645695	1,2	oropharynx posterior airway
Female 6 to Male 10	0.0467217	3, 13, 21	Lateral pharyngeal recesses anterior superior airway
Female 7 to Male 6	0.0140127	18, 21	Lateral pharyngeal recesses superior airway
Female 8 to Male 2	0.051236	6, 18, 21	Lateral pharyngeal recesses
Female 9 to Male 4	0.0902966	18	N/A*
Female 10 to Male 3	0.149947	21	Posterior superior airway

*N/A, not applicable

APPENDIX B. FIGURES

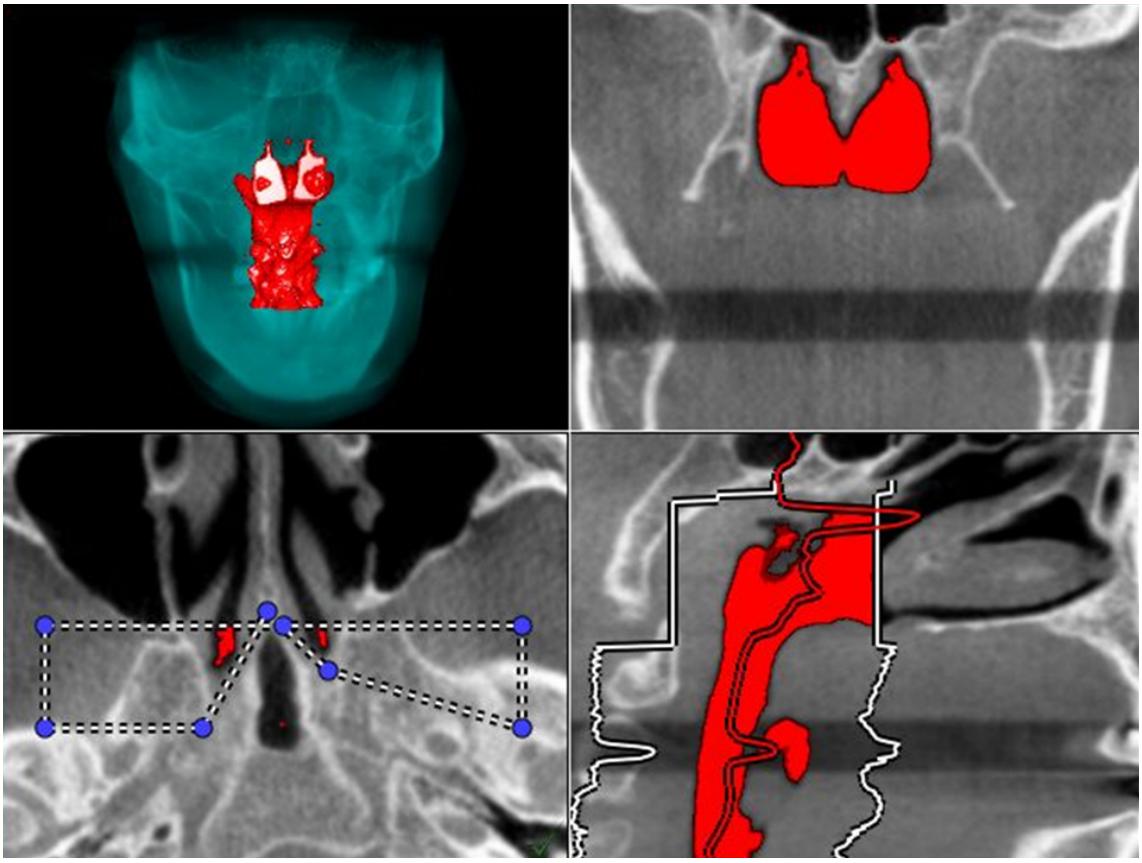

Figure 1. Automatic airway boundary- extraction of Airway3D

Anterior view of segmented airway model at ideal threshold may be visualized with accompanying CBCT volume (top left). The segmented airway is highlighted red and shown in coronal (top right), transverse (bottom left), and sagittal (bottom right) views of CBCT scans. PCA axis identifies the middle of the airway, as shown by red dot (bottom left) and white lines indicate automatic airway extraction boundaries (bottom left and right) that may also be manually adjusted to include only the volume of interest.

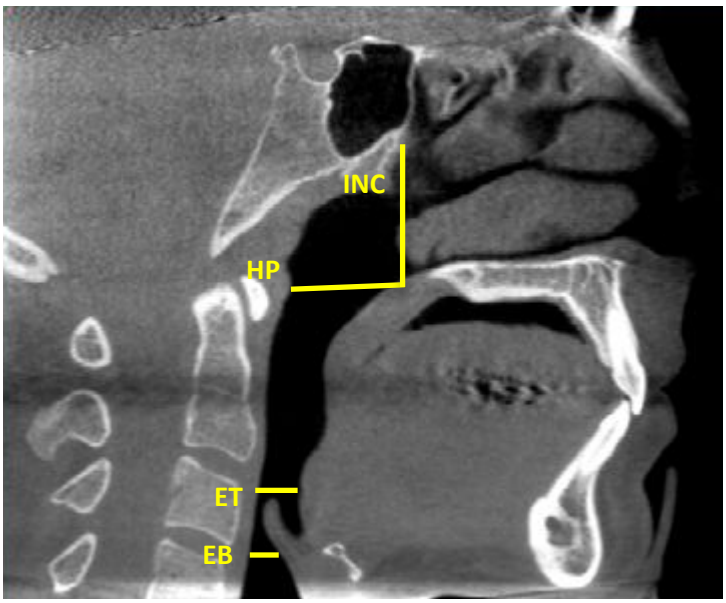

Figure 2. User-defined airway boundaries

User-defined airway boundaries for upper airway segmentation are shown in yellow in a parasagittal view. Boundaries include the hard palate (HP), tip of the epiglottis (ET), base of the epiglottis (EB), and the most posterior point of the more anterior right or left inferior nasal conchae (INC). Automatically defined boundaries include the superior, anterior, posterior, and lateral walls of the pharynx.

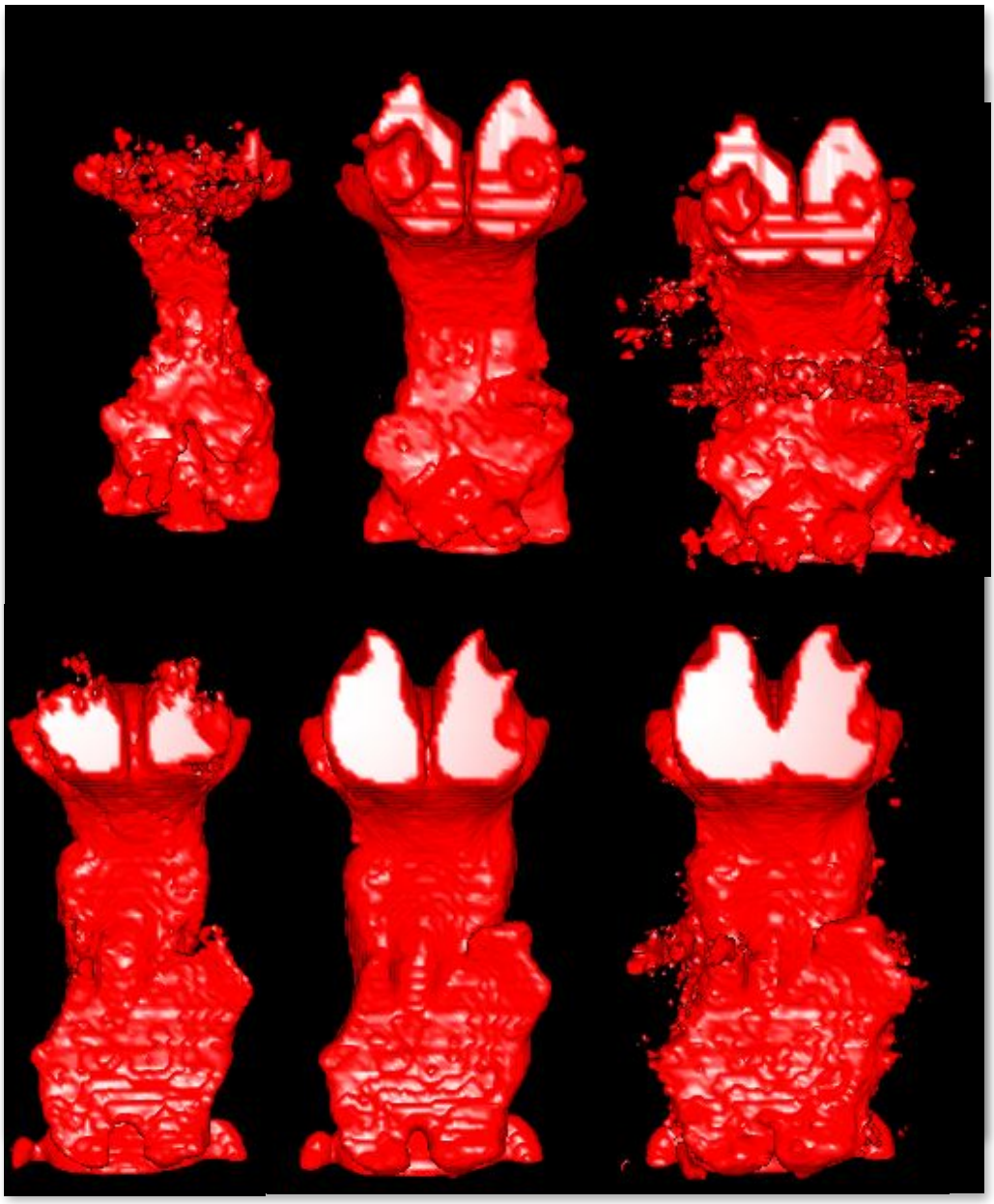

Figure 3. Automatic airway segmentation of Airway3D

Anterior views of female 7(top row) and male 1 (bottom row) automatically segmented airway models with threshold level 5 (left), ideal threshold level 45 for female 1 and 50 for male 1 (middle), and threshold level 80 (right). All models were segmented with GF level 3. Automatic airway segmentation at threshold level 5 renders incomplete airway models, while segmentation

at threshold level 80 shows excessive model construction, excessive airway volume, and inclusion of soft tissues.

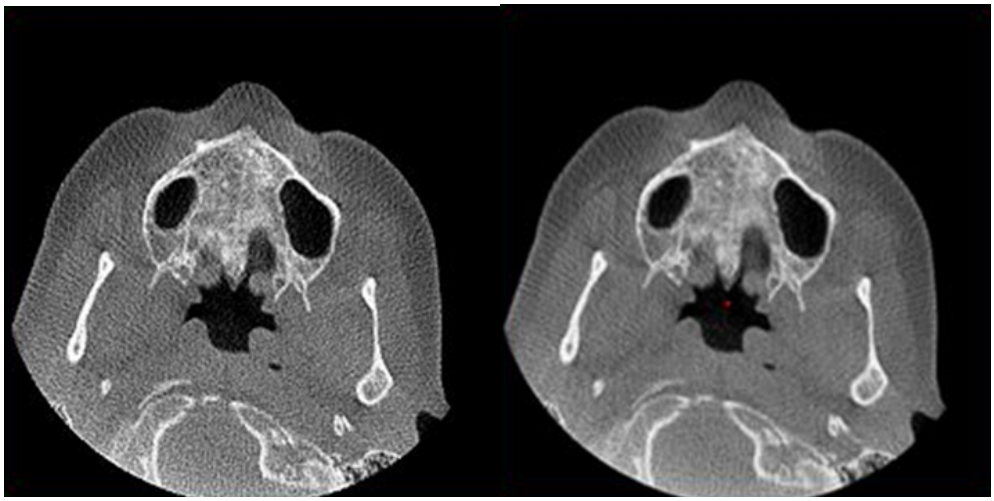

Figure 4. Gaussian Filter smoothing

GF is used to blur the image providing a more consistent pixel interview facilitating automatic edge detection. Non-GF (left) appears less smooth with less defined airway edges than GF level 3 (right) images.

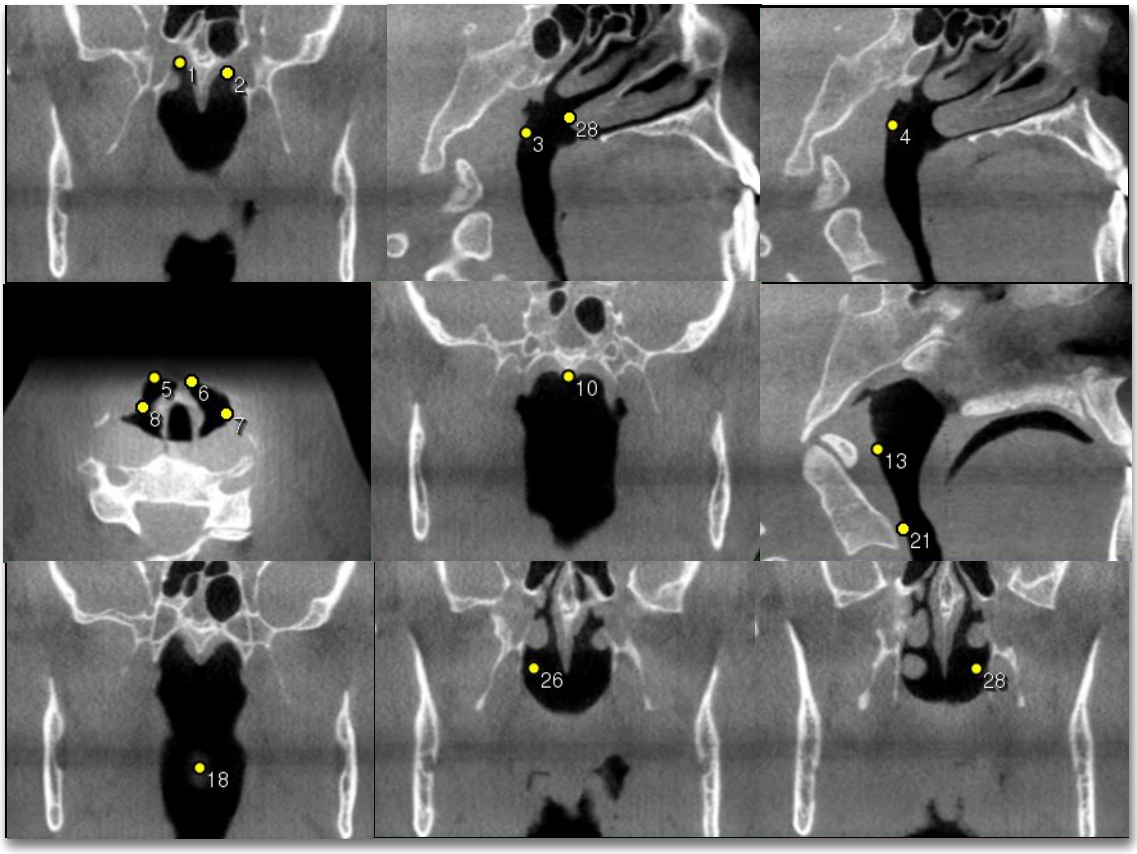

Figure 5. Landmarks manually identified on CBCT scans

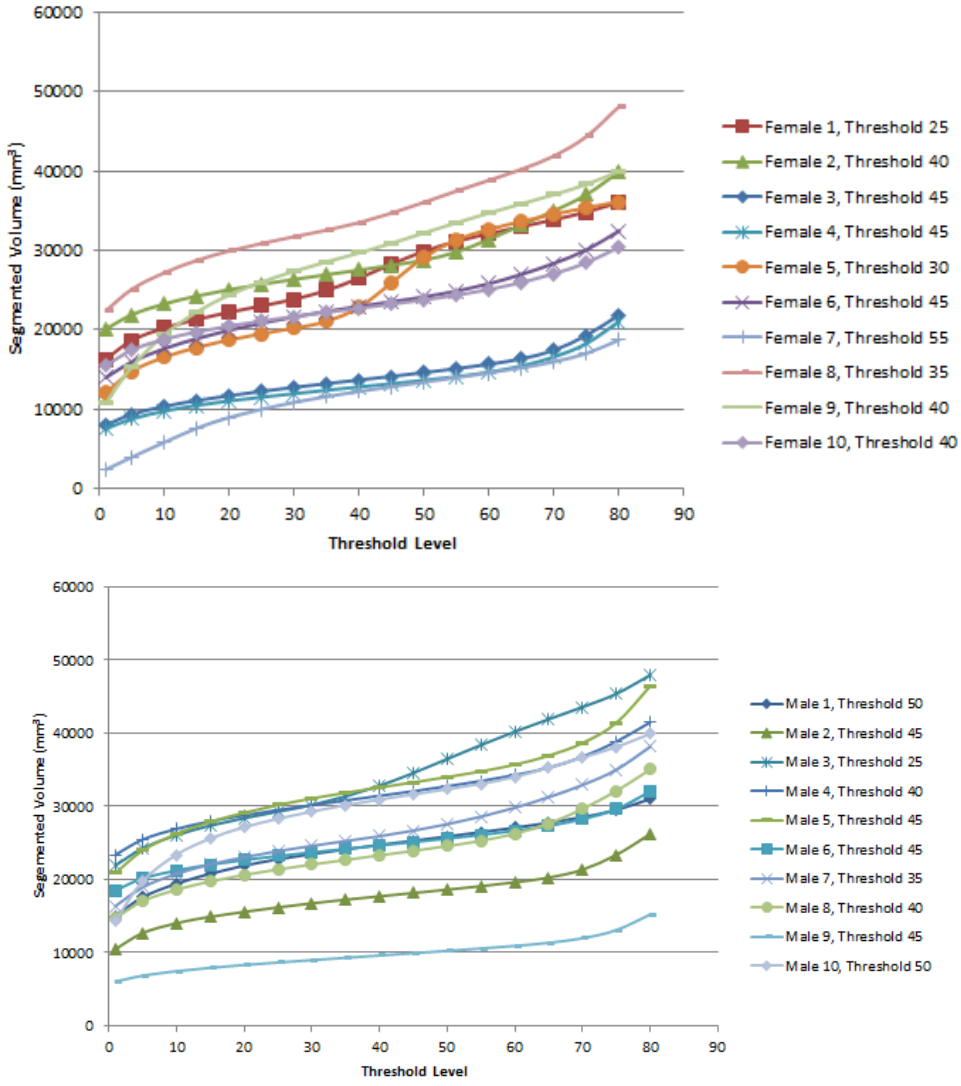

Figure 6. Individual female and male segmented volumes

Individual female (top) and individual male (bottom) airway segmented volumes at modified threshold values 5 through 80 pixels. Ideal thresholds were found at plateaus, showing smallest changes in airway volume. Ideal thresholds, selected for segmenting representative airway models, are listed in legends.

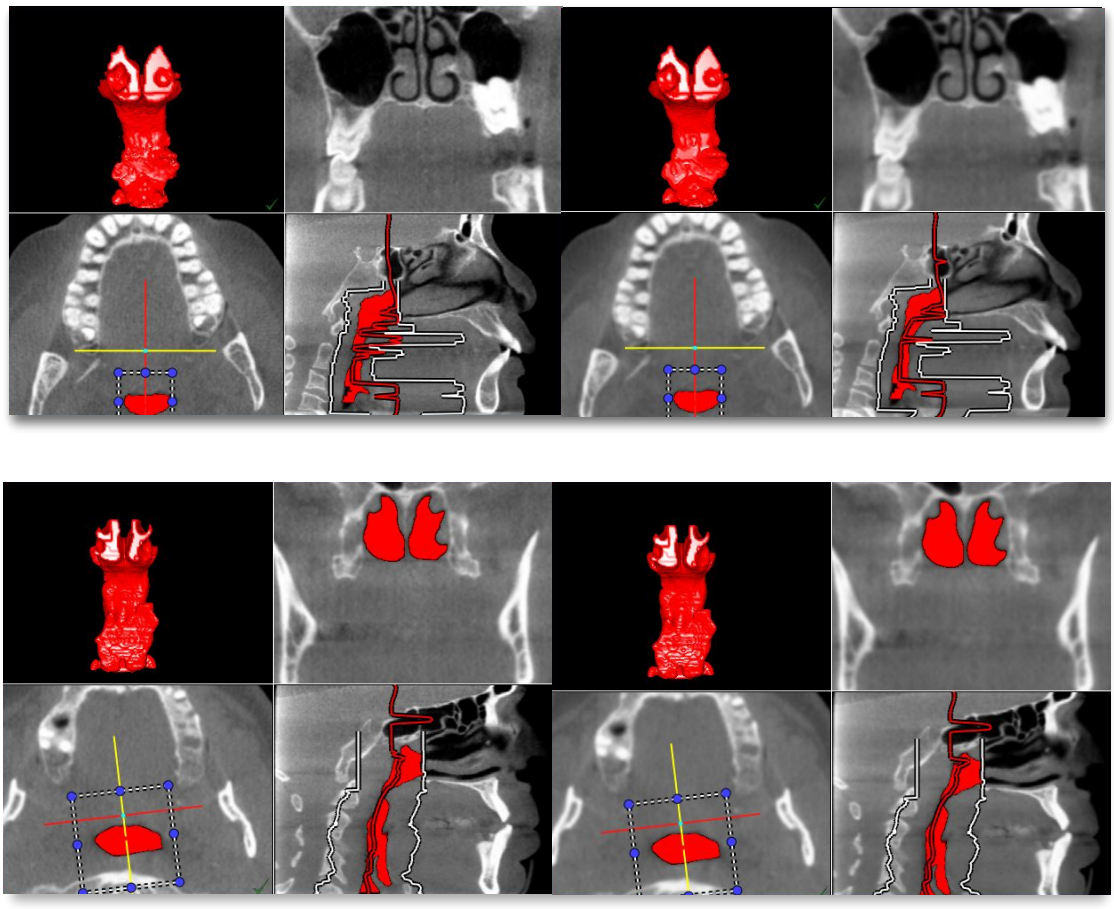

Figure 7. Gaussian Filter smoothing from levels 2 through 10

Randomly selected Female 7 (top quads) and Male 1 (bottom quads) with altered GF levels 2 (left quads) and 10 (right quads), at ideal thresholds 55 and 50, respectively, show as GF increased, CBCT slices became increasingly blurred. PCA axes determining the center of the airway became increasingly altered and linear and models became slightly smoothed, as GF level increased. Segmented volume increased and model surface area decreased slightly from GF levels 2 to 10.

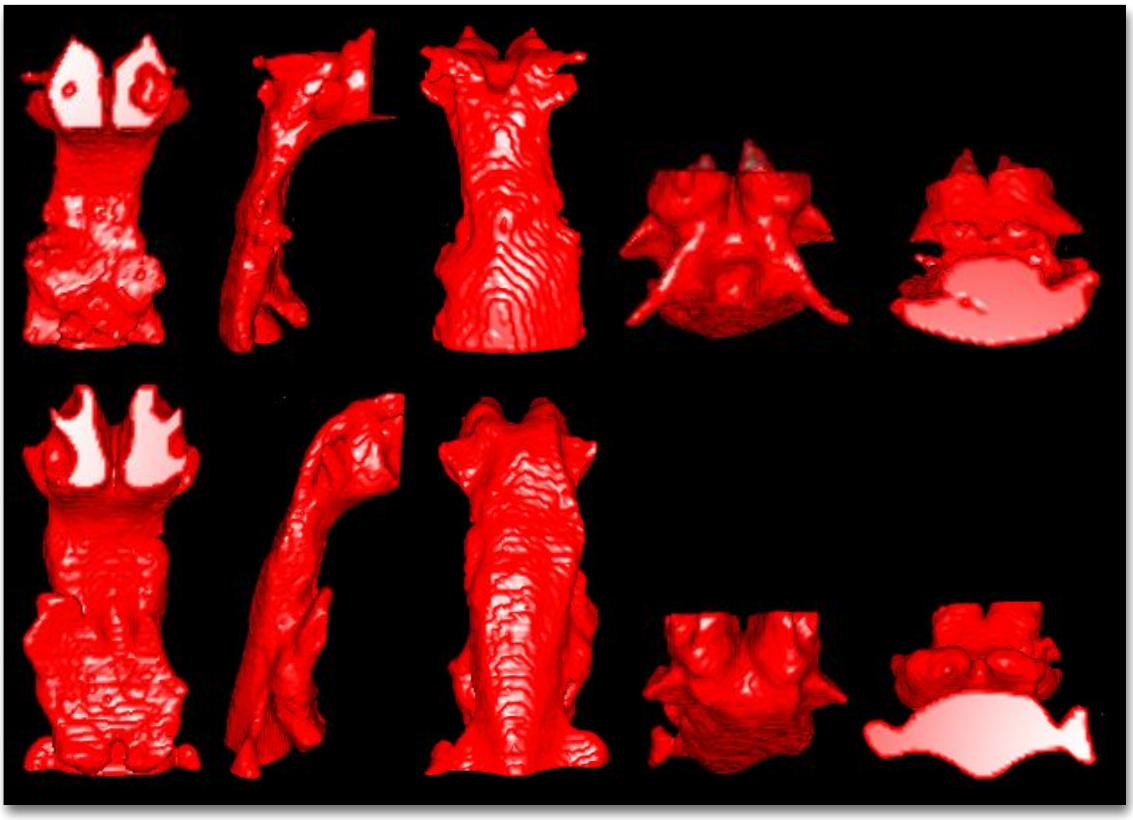

Figure 8. Representative female and male airway models

Anterior, right lateral, posterior, superior, and inferior views of example female 7 airway model (top) and Male 1 airway model (bottom) show inclusion of expected features, and models include the entire desired airway and exclude sinuses.

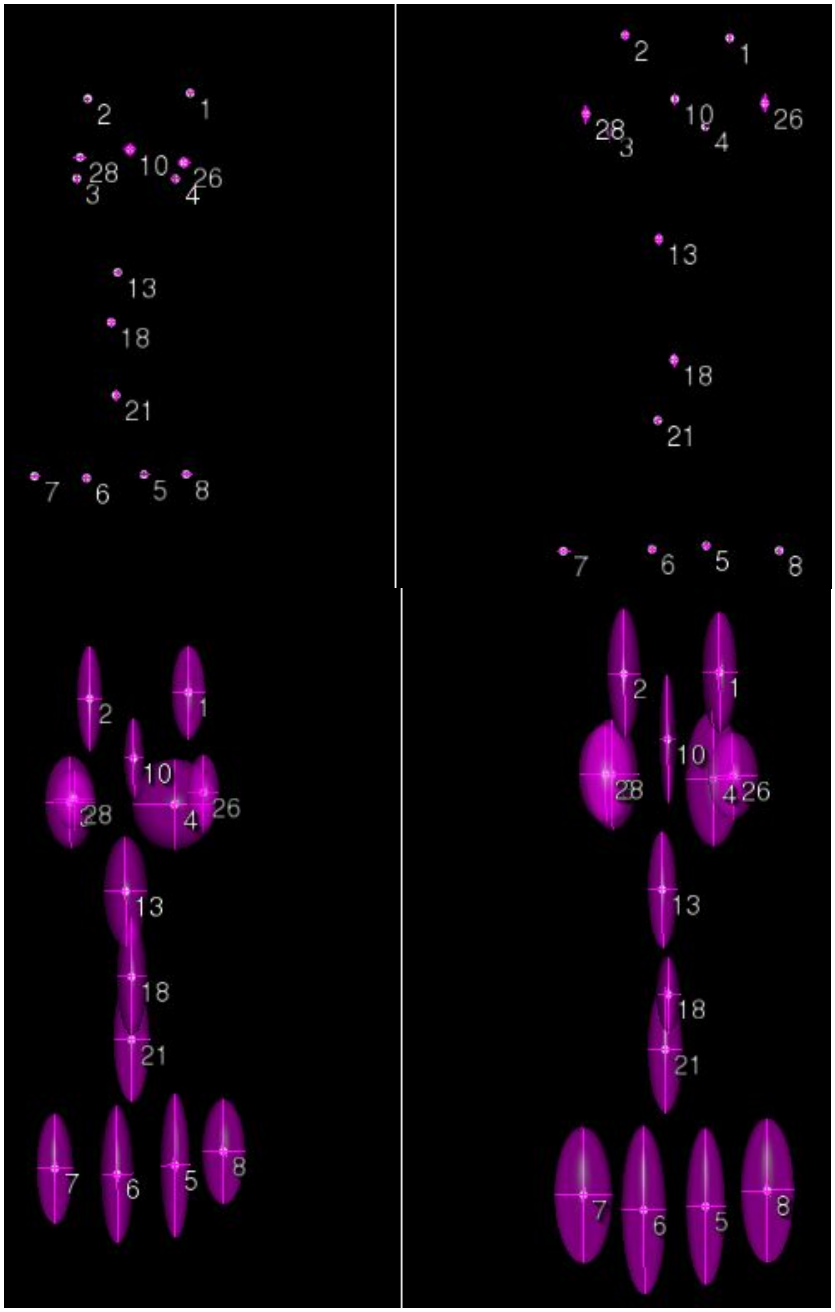

Figure 9. Procrustes Superimposition for user reliability

Procrustes analysis measures variance around landmarks and is visualized by small purple spheres for examples repeated landmarks for female 1 (top left) and repeated landmarks for male 1 (top right) and large purple spheres for all female models (bottom left) and all male models (bottom right). Models can be visualized in anterior view (shown above) and rotated.

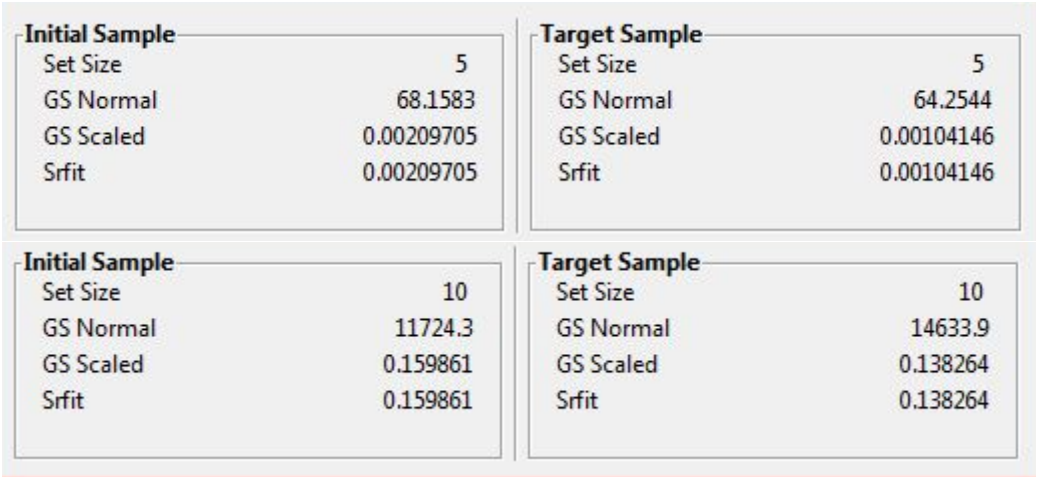

Figure 10. Srfit results of Procrustes Superimposition for user reliability

Example Srfit results for replicate .fem model for female 7 (top left), male 1 (top right), all females (bottom left), and all males (bottom right) show Srfit is smaller for replicate .fem models than Srfit of groups.

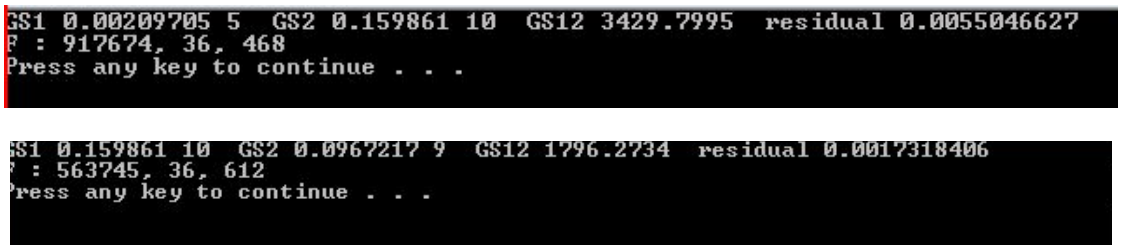

Figure 11. Gsf of shape within a female and male

Example *F* analysis for replicate female 7 to all females (top) and replicate male 1 to all males, excluding male 9, (bottom) show large and significant F values.

lambda =

214.841
48.9789
31.9618
15.2907
8.04601
3.24512

loadings =

0.661471	-0.250248	0.0885423	-0.130608	0.432606	-0.536457
0.678573	0.230575	0.32644	0.0792321	-0.262868	0.551755
0.0470338	-0.626878	-0.0728301	-0.611114	-0.461274	0.115208
0.101575	-0.145889	0.0206135	0.562155	-0.656725	-0.469754
0.120674	-0.533649	-0.473497	0.495934	0.256616	0.405778
0.273684	0.430315	-0.809734	-0.203063	-0.183957	-0.0958252

eigenspace projected (plotted) =

Female1A:	-15.1542	-2.64891	-1.55905	4.13375	-5.0761	0.836523
Female2:	-0.0153826	4.7076	3.43343	0.688021	2.48454	4.09359
Female3off1034:	0.247881	-4.10093	7.63087	-7.20705	-1.4926	-2.38175
Female4:	-13.1494	-0.949368	0.965523	-2.75539	0.448741	2.45323
Female5:	-12.0404	-6.95171	-6.13093	-3.13502	2.8121	0.174645
Female6:	-4.45564	-9.76576	9.73503	5.11107	-0.938907	-1.08503
Female7A:	-25.767	7.72969	-10.1514	-0.472337	-2.76588	-1.80631
Female8:	7.75535	-7.41847	5.57126	-0.745012	2.11927	-0.241398
Female9:	4.49691	4.13511	-6.10668	0.123533	2.99269	-2.16025
Female10:	-0.860729	10.7553	3.29638	-4.36458	-2.26968	0.501812
Male1A:	-1.14705	-0.102745	4.45325	2.83134	-4.27732	-0.0123263
Male2:	-3.53911	0.876087	-1.18966	-6.78757	-1.61146	-0.478651
Male3:	8.61104	14.5534	1.72251	5.59078	2.5888	0.683743
Male4:	4.16825	-1.60912	1.73765	3.75355	-2.19255	-1.08254
Male5:	21.2169	-13.0768	-13.2486	1.35001	-1.73873	2.29272
Male6:	22.7649	8.43388	-0.512799	-3.38172	-1.3146	0.994625
Male7:	11.3204	-4.85763	2.84407	-3.3257	1.87051	1.30272
Male8:	14.5063	-0.660783	-2.6214	0.896835	4.09786	-3.44958
Male9:	-33.743	-1.83305	0.869656	2.531	5.04152	0.439884
Male10:	14.7838	2.78428	-0.739037	5.16449	-0.778204	-1.07565

input data matrix (20 x 6) =

Female1A:	68.5137	67.3659	19.073	20.1246	39.2656	20.1453
Female2:	79.1022	80.5012	13.8033	12.2597	36.3557	22.4083
Female3off1034:	84.6367	76.8662	24.9451	14.8735	31.5371	18.2464
Female4:	72.0606	68.8361	19.7659	11.8718	36.0624	19.6087
Female5:	75.9622	63.9795	22.9769	12.0187	42.2532	22.9363
Female6:	81.0644	74.6011	20.488	21.2174	39.7735	10.0902
Female7A:	61.1544	57.322	14.1382	14.4903	33.751	29.4279
Female8:	89.8208	81.2668	22.1594	16.3328	40.1888	18.3595
Female9:	85.034	76.688	14.4593	14.8916	39.0358	31.7423
Female10:	77.5475	80.1449	14.8492	13.2578	27.9081	27.1351
Male1A:	78.6452	78.6389	18.0275	20.4419	35.965	20.405
Male2:	78.9781	73.6792	22.3072	13.0008	33.5504	26.2483
Male3:	83.427	86.5462	4.7244	15.9537	34.0272	29.7034
Male4:	83.6532	79.9465	17.771	20.7976	39.2542	22.9422
Male5:	95.1728	85.5316	28.5016	20.6587	54.8213	34.8894
Male6:	93.4393	94.4967	16.7087	15.6115	34.734	35.264
Male7:	90.6978	84.0991	22.7901	14.2524	39.8266	23.0673
Male8:	94.2325	82.5714	16.5517	16.9944	41.2966	29.359
Male9:	61.0277	52.7275	13.7772	10.8083	37.0776	11.9446
Male10:	89.7802	87.0982	14.1827	21.045	40.4288	29.1961

Figure 12. PCA table of Male 9 linear measurements

Lambda (top) lists PCA axes in order of increasing variance. Loadings (second to top) lists measurement variance (rows) for each PCA axis (columns). Eigenspace projected (second to bottom) lists plot points for each participant. Input data matrix (bottom) lists Male 9 measurements in a row.

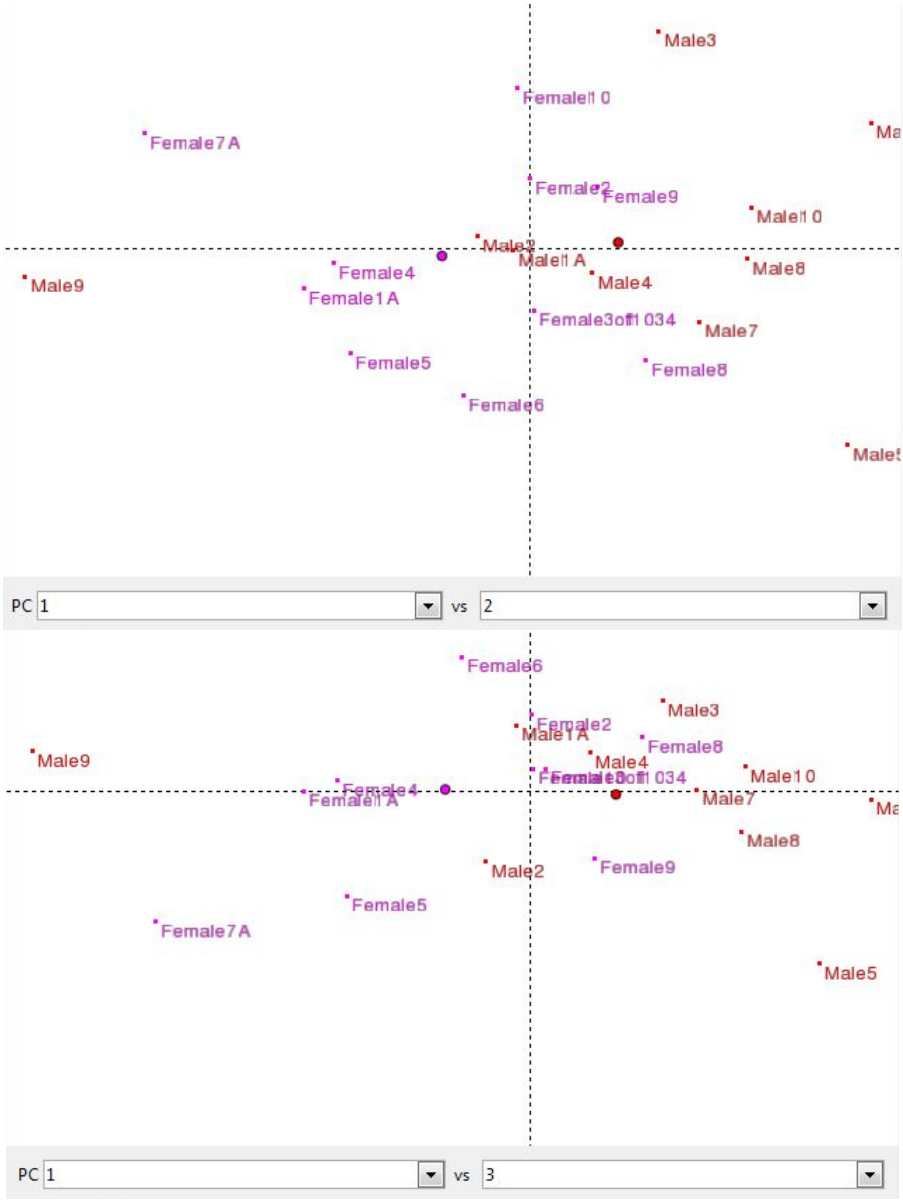

Figure 13. Graphs of PCA Axes 1 to 2 and 3 comparing females to males

PCA axes 1 by 2 (above) and PCA axes 1 by 3 (bottom) show clustering of females and males. Male 9 is observed to the far left of the plot, away from both female and male clusters.

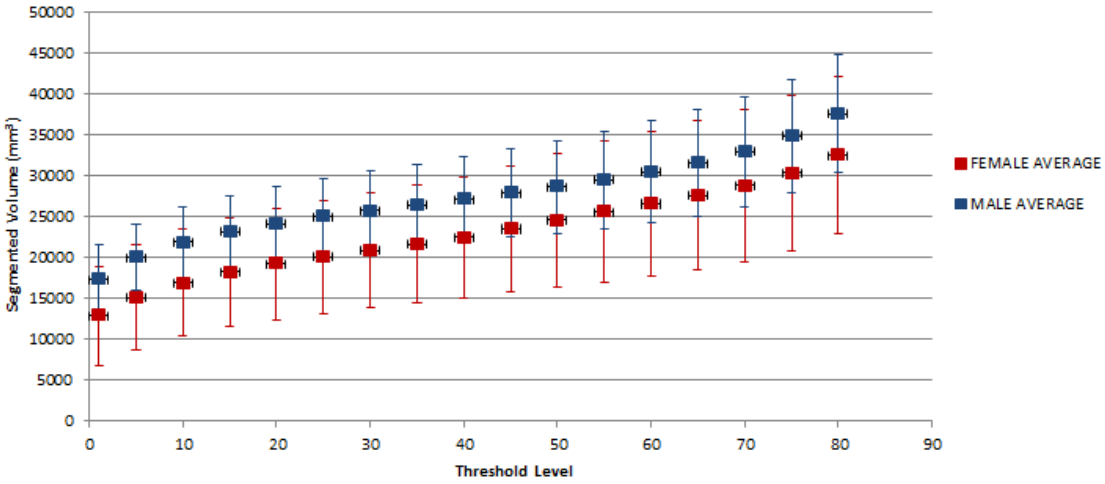

Figure 14. Average female and male airway segmented volumes

Average female AV (red) compared to average male AV, excluding Male9, (blue) shows males have a larger AV than female AV.

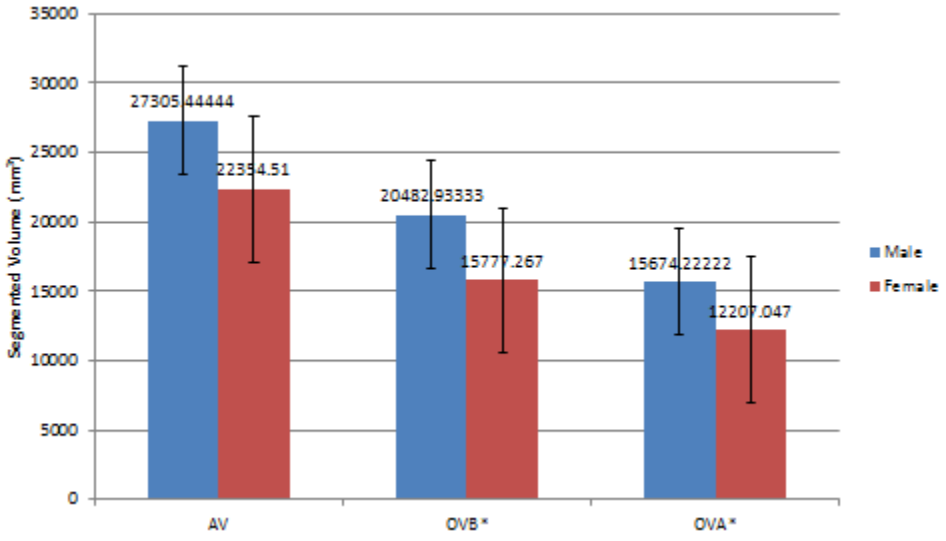

Figure 15. Average male and female airway volume at threshold

Male and female airway volume averages, excluding Male 9, of nasopharynx to EB (left), HP to EB (middle), and HP to ET (right) listed at the top of each graph. Bars indicate one standard deviation above and below the mean.*Significantly different between males and females, $p<.05$.

lambda =

271.366
0.578476
0.206323
0.100364
0.0553145
0.0266932

loadings =

0.578374	-0.0736395	0.301414	0.0348547	-0.722884	-0.213153
0.714899	0.172055	-0.206998	0.395929	0.505739	-0.0627418
0.126889	-0.775727	-0.57627	-0.177375	-0.0289972	-0.133254
0.216888	-0.313115	0.277717	-0.047588	0.0598599	0.878604
0.0762335	-0.343592	0.641538	-0.30822	0.464329	-0.392379
-0.292319	-0.38357	0.213346	0.84457	-0.0405175	-0.0834665

eigenspace projected (plotted) =

Female7A:	-14.9074	0.592845	0.0388832	0.443544	0.00733697	0.322057
Female7B:	-16.3385	0.237148	0.390939	0.378036	0.11416	-0.189454
Female7C:	-16.4334	-0.608656	0.587228	-0.318712	-0.364302	-0.0179906
Female7D:	-15.0454	-1.05047	-0.477244	0.0498507	0.0593104	-0.144341
Female7E:	-15.3575	0.785573	-0.589047	-0.541413	0.202216	0.0434846
Male1A:	15.039	0.792244	-0.194763	0.217186	-0.218619	-0.148454
Male1B:	14.8939	0.812565	0.603917	-0.325139	0.0473576	-0.0103159
Male1C:	16.0372	-1.15658	0.213803	-0.0450468	0.19038	0.197064
Male1D:	16.2406	-0.206031	0.00473795	0.0981592	0.313211	-0.113324
Male1E:	15.8714	-0.198634	-0.578454	0.0435349	-0.351051	0.061273

input data matrix (10 x 6) =

Female7A:	61.1544	57.322	14.1382	14.4903	33.751	29.4279
Female7B:	60.4885	56.225	14.1064	13.9492	34.2605	30.0408
Female7C:	60.8401	55.4424	14.752	14.4031	34.5951	29.8515
Female7D:	61.0881	56.9471	15.8234	14.4437	34.3025	29.6928
Female7E:	60.5747	56.8894	14.4997	13.9718	33.751	28.5351
Male1A:	78.6452	78.6389	18.0275	20.4419	35.965	20.405
Male1B:	78.5599	78.2845	17.6031	20.7889	36.6958	20.1296
Male1C:	79.1107	79.014	19.4191	21.7226	37.108	20.681
Male1D:	79.0778	79.5045	18.8404	21.1388	36.7974	20.3542
Male1E:	79.129	78.9941	19.1296	21.0107	36.0325	20.301

Figure 16. PCA Table of replicate F7 to replicate M1

Linear measurements analyzed include LA, LB, LATA, LATB, APA, and APB, listed in order.

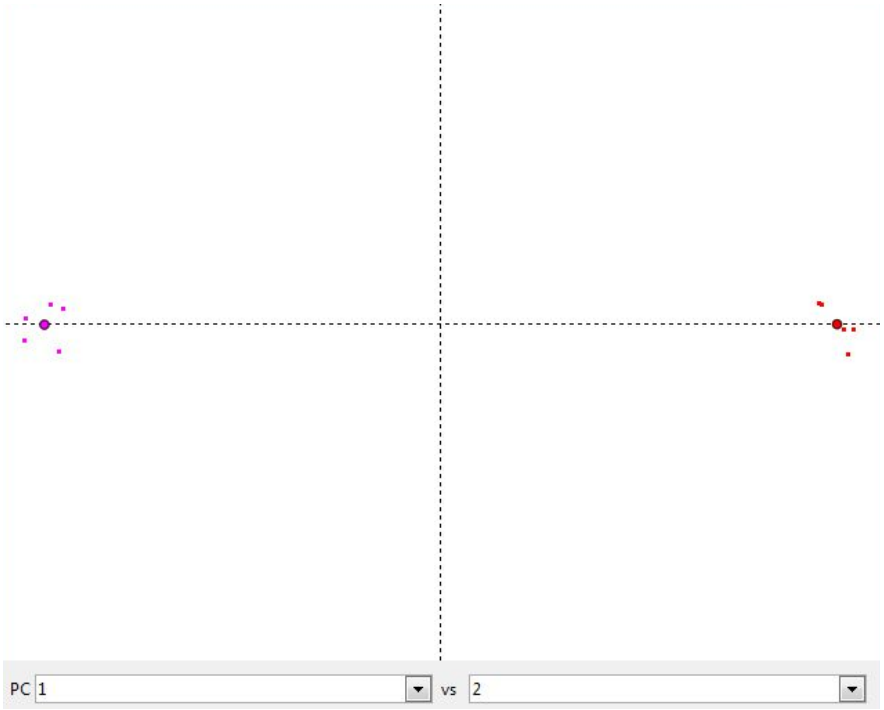

Figure 17. PCA plot of PCA axes 1 and 2 comparing replicate F7 to replicate M1

lambda =

161.147
51.4059
33.6765
15.7161
6.23533
3.39527

loadings =

0.688992	-0.223108	0.077995	-0.191464	0.410973	0.513686
0.66203	0.250675	0.318724	0.0885175	-0.33465	-0.526751
0.0166816	-0.641077	-0.0563738	-0.55036	-0.52614	-0.076449
0.0806883	-0.149074	0.024413	0.635855	-0.557066	0.506001
0.166748	-0.522129	-0.480086	0.457659	0.276389	-0.428078
0.228938	0.426103	-0.811218	-0.197096	-0.235741	0.116311

eigenspace projected (plotted) =

Female1A:	-16.9648	-3.3176	-1.26239	5.25107	-3.15817	-0.769258
Female2A:	-1.66306	4.64714	3.41628	0.508005	2.61382	-4.31709
Female3:	-1.61591	-4.28876	7.81461	-6.72848	-1.56412	2.49013
Female4:	-14.859	-1.51043	1.21539	-2.28701	1.28145	-2.64181
Female5:	-13.5265	-7.49326	-5.87709	-2.96035	3.66547	-0.513609
Female6:	-5.63305	-9.92376	9.88251	5.61885	0.736011	0.924549
Female7A:	-28.016	6.64477	-9.7797	0.550994	-0.798902	1.70767
Female8:	6.40906	-7.24305	5.56888	-0.933226	2.11107	0.0960636
Female9A:	2.7065	4.13286	-6.16769	-0.265927	3.05676	1.95861
Female10:	-3.19862	10.5102	3.36804	-3.96465	-2.46137	-0.336884
Male1A:	-3.00397	-0.295146	4.56144	3.52451	-3.36704	0.180651
Male2A:	-5.65201	0.503535	-0.997319	-6.32183	-1.72186	0.585094
Male3:	6.74708	14.7914	1.48225	5.05702	2.72384	-0.871196
Male4:	2.4659	-1.6096	1.75462	4.05398	-1.49873	1.15111
Male5A:	19.5991	-12.6753	-13.3405	1.11842	-2.71578	-2.03834
Male6:	20.4721	8.91909	-0.737002	-3.74195	-3.05231	-0.661025
Male7:	9.7484	-4.62781	2.80846	-3.61404	1.14083	-1.34365
Male8:	12.9751	-0.295455	-2.79376	0.183566	3.78256	3.24367
Male10A:	13.0098	3.13119	-0.917007	4.95104	-0.773515	1.15532

input data matrix (19 x 6) =

Female1A:	68.5137	67.3659	19.073	20.1246	39.2656	20.1453
Female2A:	79.1022	80.5012	13.8033	12.2597	36.3557	22.4083
Female3:	84.6367	76.8662	24.9451	14.8735	31.5371	18.2464
Female4:	72.0606	68.8361	19.7659	11.8718	36.0624	19.6087
Female5:	75.9622	63.9795	22.9769	12.0187	42.2532	22.9363
Female6:	81.0644	74.6011	20.488	21.2174	39.7735	10.0902
Female7A:	61.1544	57.322	14.1382	14.4903	33.751	29.4279
Female8:	89.8208	81.2668	22.1594	16.3328	40.1888	18.3595
Female9A:	85.034	76.688	14.4593	14.8916	39.0358	31.7423
Female10:	77.5475	80.1449	14.8492	13.2578	27.9081	27.1351
Male1A:	78.6452	78.6389	18.0275	20.4419	35.965	20.405
Male2A:	78.9781	73.6792	22.3072	13.0008	33.5504	26.2483
Male3:	83.427	86.5462	4.7244	15.9537	34.0272	29.7034
Male4:	83.6532	79.9465	17.771	20.7976	39.2542	22.9422
Male5A:	95.1728	85.5316	28.5016	20.6587	54.8213	34.8894
Male6:	93.4393	94.4967	16.7087	15.6115	34.734	35.264
Male7:	90.6978	84.0991	22.7901	14.2524	39.8266	23.0673
Male8:	94.2325	82.5714	16.5517	16.9944	41.2966	29.359
Male10A:	89.7802	87.0982	14.1827	21.045	40.4288	29.1961

Figure 18. PCA Table of females and males

Linear measurements analyzed include LA, LB, LATA, LATB, APA, and APB, listed in order, for all participants excluding Male 9.

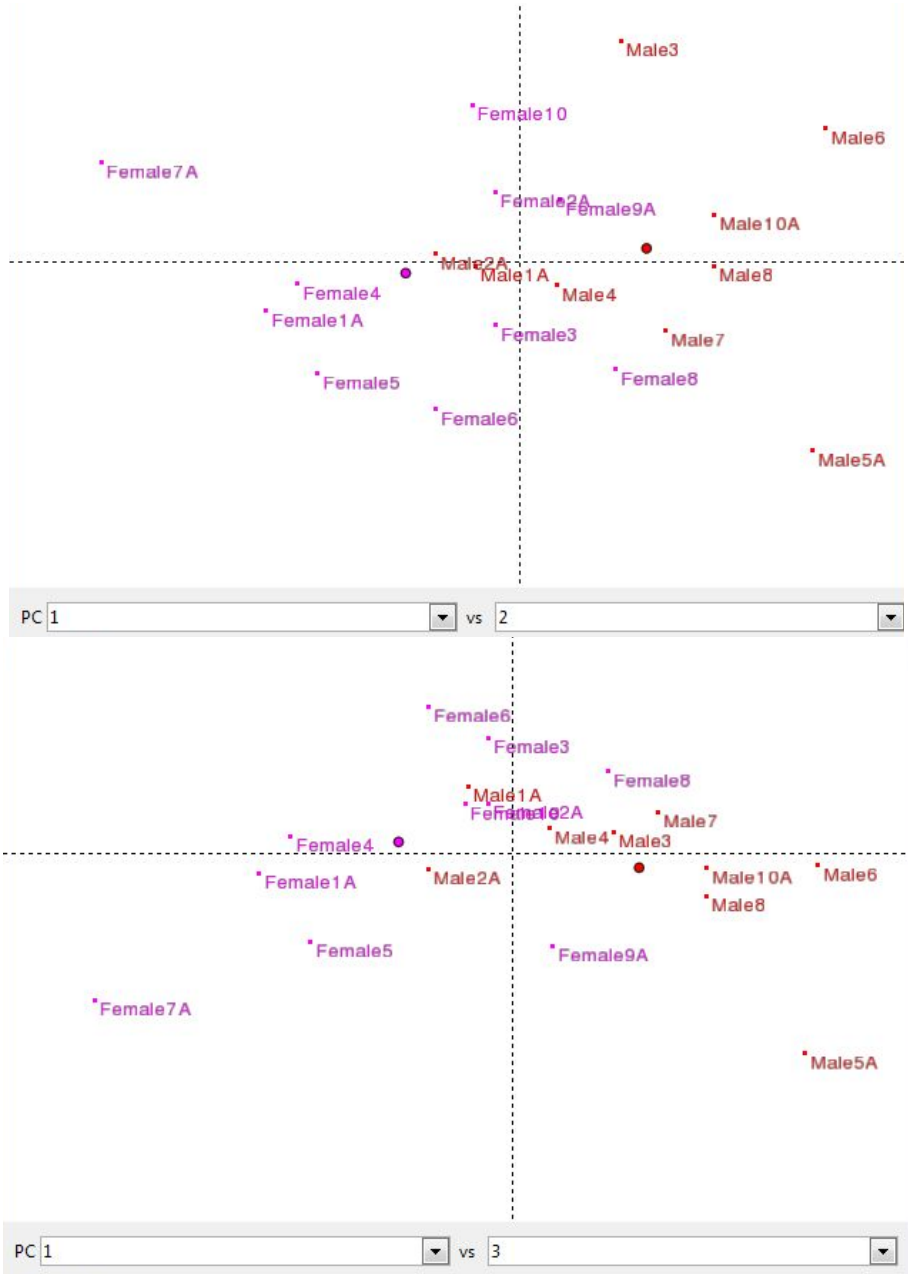

Figure 19. Graphs of PCA Axes 1 to 2 and 3 comparing females to males

PCA axes 1 by 2 (above) and PCA axes 1 by 3 (bottom) show clustering of females and males.

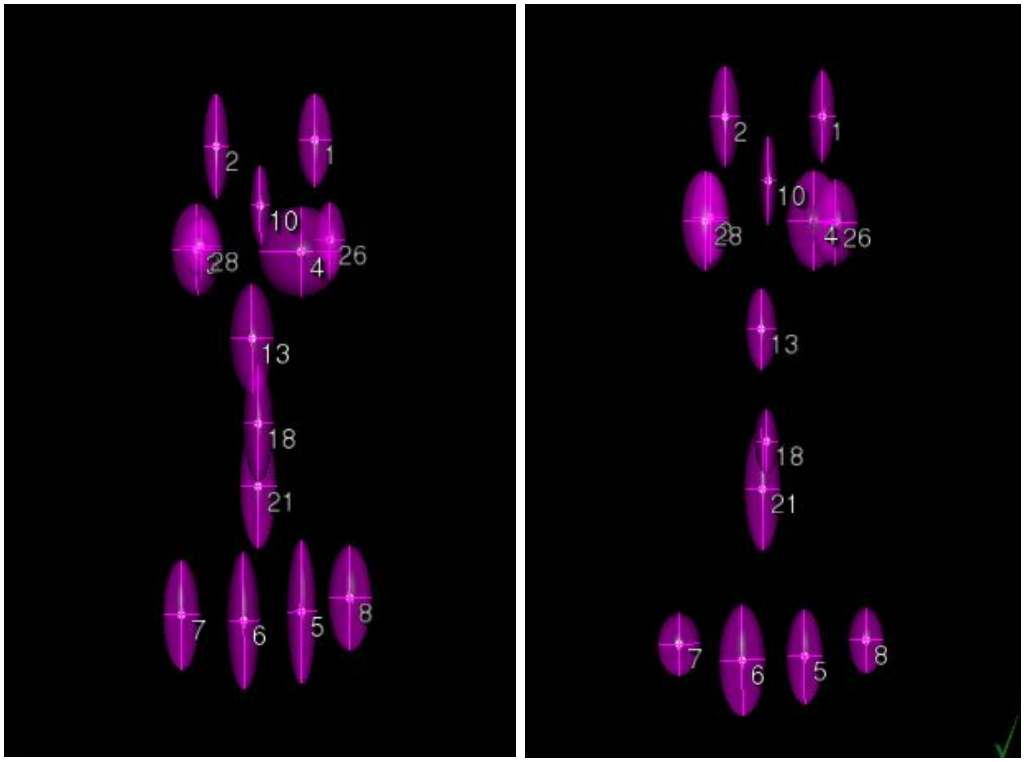

Initial Sample	
Set Size	10
GS Normal	11724.3
GS Scaled	0.159861
Srfit	0.159861

Target Sample	
Set Size	9
GS Normal	7990.18
GS Scaled	0.0967217
Srfit	0.0967217

Figure 20. Procrustes Superimposition comparing females to males

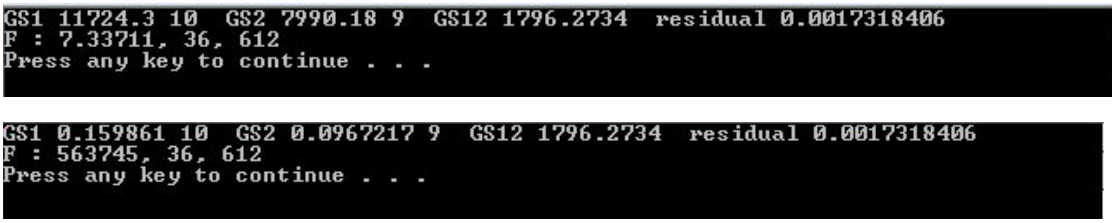

Figure 21. Gsf of size and shape between females and males

Gsf comparing females and males for size (top) showed a small but significant F value, and gsf comparing females and males for shape (bottom) showed a large and significant F value, quantitatively showing that there size and shape differences exist between male and female airways.

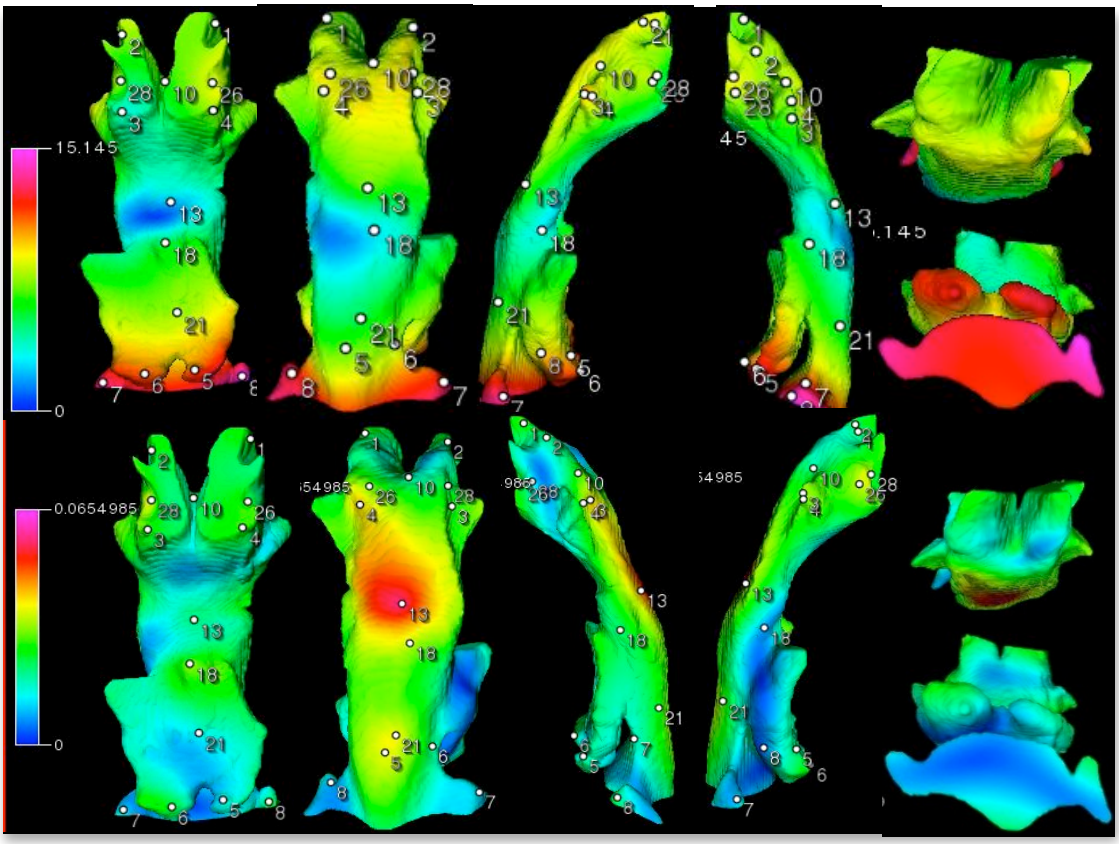

Figure 22. DCA of a female into a male

Example DCA of Female 7 is warped into Male1 target model for size (top row) and shape (bottom row), creating a colored warped model of Male 1. Few, isolated hot spots were located in anterior, right lateral, posterior, superior, and inferior views of Male 1 warped- initial model (left to right).

REFERENCES

Abramson, Z.R., Susarla, S., Tagoni, J.R., & Kaban, L. (2010). Three-dimensional computed tomographic analysis of airway anatomy. *Journal of Oral and Maxillofacial Surgery, 68*, 363-371.

Abramson, Z.R., Susarla, S., Troulis, M., & Kaban, L. (2009). Age-related changes of the upper airway assessed by 3-dimensional computed tomography. *Journal of Craniofacial Surgery, 20(1),* 657-663.

Ahmadi, N., Shapiro, G.K., Chung, S.A., Shapiro, C.M. (2008). Clinical diagnosis of sleep apnea based on a single night of polysomnography vs. two nights of polysomnography. *Sleep and Breathing, 13*, 221-226.

AlGhanim, N., Comondore, V.R., Fleetham, J., Marra, C.A., & Ayas, N.T. (2008). The economic impact of obstructive sleep apnea. *Lung, 186*, 7-12.

American Academy of Sleep Medicine. (2001). *The International Classification of Sleep Disorders, Revised: Diagnostic and Coding Manual*. Retrieved from http://www.aasm.org/PDF/ICSD.pdf.

Ayas, N.T., Fox, J., Ryan, C.F., & Fleetham, J.A. (2010). Initial use of portable monitoring versus polysomnography to confirm obstructive sleep apnea in symptomatic patients: an economic decision model. *Sleep*, *11*, 320-324.

Bailey, E.F. (2011). Activities of human genioglossus motor units*. Respiratory Physiology and Neurobiology*. Electronic publication ahead of print.

Bailey, E.F., Huang, Y., & Fregosi, R.F. (2006). Anatomic consequences of intrinsic tongue muscle activation. *Journal of Applied Physiology, 101*, 1377-1385.

Bailey, E.F., & Fregosi, R.F. (2006). Modulation of upper airway muscle activities by bronchopulmonary afferents. *Journal of Applied Physiology*, *101*, 609-617.

Barnes, M., Goldsworthy, U.R., Cary, B.A., & Hill, C.J. (2009). A diet and exercise program to

improve clinical outcomes in patients with obstructive sleep apnea: a feasibility study. *Journal of Clinical Sleep Medicine, 5(5)*, 409-415.

Bookstein, F.L. (1996). Biometrics, biomathematics and the morphometric synthesis. *Bulletin of Mathematical Biology, 58(2),* 313-365.

Bookstein, F.L. (1997). Landmark methods for forms without landmarks: morphometrics of group differences in outline shape. *Medical Image Analysis, 1(3),* 225-243.

Bookstein, F.L., Slice, D.E., Gunz, P., & Mitteroeker, P. (2004). Anthropology takes control of morphometrics. *Collegium Antropologicum, 28*, Supplement 2, 121-32.

Caples, S., Gami, A., & Somers, V. (2005). Obstructive Sleep Apnea. *Focus, 3(4),* 557-567.

Cevidanes, L.H.S., Styner, M.A., & Proffit, W.R. (2006). Image analysis and superimposition of 3-dimensional cone-beam computed tomography models. *American Journal of Orthodontics and Dentofacial Orthopedics, 129*, 611-618.

Celenk, M., Farrell, M.L., Eren, H., Kumar, K., Singh, G.D., & Lozanoff, S. (2010). Upper airway detection and visualization from cone beam image slices. *Journal of X-ray Science and Technology,18(2),* 121-135.

Chenin, D.L. (2010). 3D cephalometrics: the new norm. *Alpha Omegan, 103(2*), 51-56.

Dahlqvist, J., Dahlqvist, A., Marklund, M., Berggren, D., Stenlund, H., & Franklin, K. (2007). Physical findings in the upper airways related to obstructive sleep apnea in men and women. *Acta Oto-Laryngologica, 127*, 623-630.

National Electrical Manufacturers Association. (2008). *DICOM: Digital Imaging and Communications in Medicine*. Rosslyn,VA.

Dyken, M.E., & Im, K.B. (2009). Obstructive sleep apnea and stroke. *Chest, 136*, 1668-1677.

El, H., & Palomo, J.M. (2010). Measuring the airway in 3 dimensions: a reliability and accuracy study. *American Journal of Orthodontics and Dentofacial Orthopedics, 137(4),* S50.e1-S50.e9.

Farrell, M.L. (2009). *Fully automatic airway segmentation on the GPU from cone-beam CT volumes*. MSc Thesis, Department of Electrical Engineering and Computer Science, Ohio University, Athens, OH.

Galetke, W., Puzzo, L., Priegnitz, C., Anduleit, N., & Randerath, W.J. (2011). Long-term therapy with continuous positive airway pressure in obstructive sleep apnea: adherence, side effects and predictors of withdrawal – a 'real life' study. *Respiration*, Electronic publication ahead of print.

Grauer, D., Cevidanes, L.S.H., & Proffit, W.R. (2009). Working with DICOM craniofacial images. *American Journal of Orthodontics and Dentofacial Orthopedics*, 136, 460-470.

Grauer, D., Cevidanes, L.S.H., Styner, M.A., Heulfe, I., Harmon, E.T., Zhu, H., & Proffit, W.R. (2010). Accuracy and landmark error calculation using cone-beam computed tomography generated cephalograms. *Angle Orthodontist, 80(2),* 286-294.

Gray, C.F. (2010). Practice-based cone-beam computed tomography: a review. *Primary Dental Care, 17(4),* 161-167.

Hassan, B., Souza, P.C., Jacobs, R., de Azumbuja, B.S., & van der Stelt, P. (2010). Influence of scanning and reconstruction parameters on quality of three-dimensional surface models of the dental arches from cone beam computed tomography. *Clinical Oral Investigations, 14*, 303-310.

Hassan, B., van der Stelt, P., & Sanderink, G. (2009). Accuracy of three-dimensional measurements obtained from cone beam computed tomography surface-rendered images for cephalometric analysis: influence of patient scanning position. *European Journal of Orthodontics, 31*, 129-134.

Holberg, C., Steinhauser, S., Geis, P., & Rudzki-Janson, I. (2005). Cone beam computed tomography in orthodontics: benefits and limitations. *Journal of Orofacial Orthopedics, 6*, 434-444.

Hutton, T.J., Buxton, B.F., & Hammond, P. (2003). Automated registration of 3D face using dense surface models. In R. Harvey & J.A. Bangham (Eds), *Proceedings of the British Machine Vision Conference* (pp. 439-448). Norwich.

In Seol, T., Chung, S., & Cho, S. (2009). 3D dense correspondence for 3D dense morphable face shape model. *International Journal of Electrical and Electronics Engineering, 3(3)*, 127-131.

Isaacs, R.S., & Sykes, J.M. (2002). Anatomy and physiology of the upper airway. *Anesthesiology Clinic of North America, 20*, 733-745.

Kakkar RK & Berry RB. 2007. Positive airway pressure treatment for obstructive sleep apnea. Chest,132(3): 1057-72.

Kranioti, E.F., Bastir, M., Sanchez-Meseguer, A., & Rosas, A. (2009).A geometric-morphometric study of the Cretan humerus for sex identification. *Forensic Science International, 189 (1-3),* 111.

Kristenson, E., Parsons, T.E., Hallgrimsson, B., & Boyd, S.K. (2008). A novel 3-D image-based morphological method for phenotypic analysis. *International Journal of Electrical and Electronics Engineering, 55(12),* 2826-2831.

Kuna, S.T. (2010). Portable-monitor testing: an alternative strategy for managing patients with obstructive sleep apnea. *Respiratory Care, 55(9),*1196-1215.

Lele, S., & Richtsmeier, J.T. (1990). Statistical models in morphometrics: are they realistic? *Systematic Zoology, 39*, 60-69.

Lenza, M.G., Lenza, M.M., Dalstra, M., Melseri, B., & Cattaneo, P.M. (2010). An analysis of different approaches to the assessment of upper airway morphology: a CBCT study. *Orthodontics and Craniofacial Research, 13(2),* 96-105.

Lopez-Jimenez, F., Kuniyoshi, F.H., Apoor, G., & Somers, V.K. (2008). Obstructive sleep apnea: implications for cardiac and vascular disease. *Chest, 133*, 793-804.

Lozanoff S, Jureczek S, Feng T, Padwal R. 1994. Anterior cranial base morphology in mice with midfacial retrusion. *Cleft Palate - Craniofacial Journal*, 31:417-428.

Maria, S., Togeiro, G.P., Chaves, C.M., Palombini, L., Tufik, S., Hora, F., & Nery, L.E. (2010). Evaluation of the upper airway in obstructive sleep apnea. *Indian Journal of Medical Research, 13*, 230-235.

McIntyre, G.T., & Mossey, P.A. (2003). Size and shape measurement in contemporary cephalometrics. *European Journal of Orthodontics, 25*, 231-242.

Mohsenin, V. (2001). Gender differences in the expression of sleep-disordered breathing:

role of upper airway dimensions. *Chest*, *120(5),* 1442-1447.

Molen, A. (2011). *The 3D Orthodontist.* Retrieved from http://3dorthodontist.com/3D_Software.html

Monteiro, L.R., Kiniz-Filho, J.A., dos Reis, S.F., & Araujo, E.D. (2002). Geometric estimates of heritability in biological shape. *Evolution, 56(3),* 53-72.

Moshiri, M., Scarfe, W.D., Hilgers, M.L., Scheetz, J.P., Silveira, A.M., & Farman, A.G. (2007). Accuracy of linear measurements from imaging plate and lateral cephalometric images derived from cone-beam computed tomography. *American Journal of Orthodontics and Dentofacial Orthopedics, 132*, 550-560.

Noel, P.B., Walczak, A.M., Xu, J., Corso, J.J., Hoffman, K.R., & Schafer, S. (2010). GPU-based cone beam computed tomography. *Computer Methods and Programs in Biomedicine, 98*, 271-277.

Oda, M., Suzuka, Y., Lan, Z., Takashima, M., Yue, Y., Kuginuki, Y., Tonami, H., & Tomoda, K. (2003). Evaluation of pharyngolaryngeal region with 3-D computed tomography. *International Congress Series, 1257,* 281-287.

Ogawa, T., Enciso, R., Shintaku, W.H., & Clark, G.T. (2007). Evaluation of cross-sectional airway configuration of obstructive sleep apnea. *Oral Surgery, Oral Medicine, Oral Pathology, Oral Radiology, and Endodontology, 103(1),* 102-108.

Oliven, A., Tov, N., Geitini, L., Steinfeld, U., Oliven, R., Schwartz, A.R., & Odeh, M. (2007). Effect of genioglossus contraction on pharyngeal lumen and airflow in sleep apnoea patients. *European Respiratory Journal, 30*, 748-758.

Osorio, F., Perilla, M., Doyle, D.J., & Palomo, J.M. (2008). Cone beam computed tomography: An innovative tool for airway assessment. *Anesthesia and Analgesia, 106*, 1803-1807.

Pavlinov, I., & Mikeshina, N.G. (2002). Principles and methods of geometric morphometrics. *Zhurnal Obshchei Biologii (Journal of General Biology), 63(6),* 473-93.

Richardson, K. (2011). Non-antibiotic treatment sore throat. *Emergency Nurse, 18(9),* 12-16.

Sagawa, M., Miyoseta, Y., Hayakawa, Y., & Honda, A. (2009). Comparison of two- and three-

dimensional filtering methods to improve image quality in multiplanar reconstruction of cone-beam computed tomography. *Oral Radiology, 25*, 154-158.

Sawani, H., Murugappan, S., Gutmark, E., Donnelly, L.F., Amin, R., Mylavarapu, G., Mihaescu, M., Khosla, S., & Kalra, M. 2010. Influence of gender on pharyngeal airway length in obese adolescents. *Annals of Otology, Rhinology, and Laryngology 119(12),* 842-847.

Schlicher, W., Nielson, I., Huang, J.C., Maki, K., Hatcher, D.C., & Miller, A.J. (2011). Consistency and precision of landmark identification in three-dimensional cone beam computed tomography scans. *European Journal of Orthodontics*. Electronic publication ahead of print.

Shi, H., Scarfe, W.C., & Farman, A.G. (2006). Upper airway segmentation and dimensions estimation from cone beam CT image datasets. *International Journal of Computer Assisted Radiology and Surgery, 1*, 177-186.

Shigeta, Y., Enciso, R., Ogawa, T., Ikawa, T., & Clark, G.T. (2008). Cervical CT derived neck fat tissue distribution differences in Japanese males and females and its effect on retroglossal and retropalatal airway volume. *Oral Surgery, Oral Medicine, Oral Pathology, Oral Radiology, and Endodontology, 106(2),* 275-284.

Shigeta, Y., Enciso, R., Ogawa, T., Shintaku, W.H., & Clark, G.T. (2008). Correlation between retroglossal airway size and body mass index in OSA and non-OSA patients using cone beam CT imaging. *Sleep and Breathing, 12*, 347-352.

Shigeta, Y., Ogawa, T., Ando, E., Clark, G.T., & Enciso, R. (2011). Influence of tongue/mandible volume ratio on oropharyngeal airway in Japanese male patients with obstructive sleep apnea. *Oral Surgery, Oral Medicine, Oral Pathology, Oral Radiology, and Endodontology, 111(2),* 239-43.

Sjosten, N., Vahtera, J., Salo, P., Oksanen, T., Saaresranta, T., Virtanen, M., Pentti, J., & Kivimaki, M. (2009). Increased risk of lost workdays prior to the diagnosis of sleep apnea. *Chest, 136*,130-136.

Susarla, S.M., Abramson, Z.R., Dodson, T.B., & Kaban, L.B. (2010). Cephalometric measurement of upper airway length correlates with the presence and severity of

obstructive sleep apnea. *Journal of Oral Maxillofacial Surgery, 68*, 2846-2855.

Sutthiprapaporn, P., Tanimoto, K., Ohtsuka, M., Nagasaki, T., Konishi, M., Iida, Y., & Katsumata, (2008). Improved inspection of the lateral pharyngeal recess using cone-beam computed tomography in the upright position. *Oral Radiology, 24*, 71-75.

Togeiro, S.M., Chaves, C.M., Palombini, L., Tufik, S., & Hora, F. (2010). Evaluation of the upper airway in obstructive sleep apnoea. *Indian Journal of Medical Research, 131*, 230-235.

Tso, H.H., Lee, J.S., Huang, J.C., Maki, K., Hatcher, D., & Miller, A.J. (2009). Evaluation of the human airway using cone beam computerized tomography. *Oral Surgery, Oral Medicine, Oral Pathology, Oral Radiology, and Endodontology, 108*, 768-776.

Vos, W., Backer, J.D., Devolder, A., Vanderveken, O., Verhulst, S., Salgado, R., Germonpre, P., Partoens, B., Wuyts, F., Parizel, P., & De Backer, W. (2007). Correlation between severity of sleep apnea and upper airway morphology based on advanced anatomical and functional imaging. *Journal of Biomechanics 40,* 2207-2213.

Walsh, J.H., Leigh, M.S., Paduch, A., Maddison, K.J., Philippe, D.L., Armstrong, J.J., Sampson, D.D., Hillman, D.R., & Eastwood, P.R. (2008). Evaluation of pharyngeal shape and size using anatomical optical coherence tomography in individuals with and without obstructive sleep apnoea. *Journal of Sleep Research 17*, 230-238.

Weir, J.P. (2005). Quantifying test-retest reliability using the intraclass correlation coefficient and the SEM. *Journal of Strength and Conditioning Research, 19(1),* 231-240.

Wellman, A., Eckert, D., Jordan, A., Edwards, B., Passaglia, C., Jackson, A., Gautam, S., Owens, R., Malhotra, A., & White, D. (2011). A method for measuring and modeling the physiological traits causing obstructive sleep apnea. *Journal of Applied Physiology, 110(6),* 1627-1637.

Young, T., Palta, M., Dempsey, J., Peppard, P., Nieto, F.J., & Hla, K.M. (2009). Burden of sleep apnea: rationale, design, and major findings of the wisconsin sleep cohort study. *Wisconsin Medical Journal, 108(5),* 246-249.

Young, T., Skatrud, J., & Peppard, P. (2004). Risk factors for obstructive sleep apnea in adults. *Journal of American Medical Association, 291(16),* 2013-2016.

Yucel, A., Unlu, M., Haktanir A., Acar, M., & Fidan, F. (2005). Evaluation of the upper airway cross-sectional area changes in different degrees of severity of obstructive sleep apnea syndrome: cephalometric and dynamic CT study. *American Journal of Neuroradiology, 26(10),* 2624-2629.